

Bound Deuteron–Antideuteron System (Deuteronium): Leading Radiative and Internal–Structure Corrections to Bound-State Energies

Gregory S. Adkins¹ and Ulrich D. Jentschura²

¹*Department of Physics and Astronomy, Franklin & Marshall College, Lancaster, Pennsylvania 17604, USA*

²*Department of Physics and LAMOR, Missouri University of Science and Technology, Rolla, Missouri 65409, USA*

We evaluate the energy levels of the deuteronium bound system, which consists of a deuteron and an antideuteron, with a special emphasis on states with nonvanishing orbital angular momenta. The excited atomic bound states of deuteronium constitute probes for the understanding of higher-order quantum electrodynamic corrections for spin-1 particles in a bound system where the typical field strength of the binding Coulomb field (at a distance of the generalized Bohr radius) exceeds Schwinger’s critical field strength. For states with nonvanishing angular momenta, effects due to the internal structure of the deuteron and virtual annihilation contributions are highly suppressed. Relevant transitions are found to be in a frequency range accessible by standard laser spectroscopic techniques. We evaluate the leading and next-to-leading energy corrections of orders $\alpha^3 m_d$ and $\alpha^4 m_d$, where α is the fine-structure constant and m_d is the deuteron mass, and also investigate internal-structure corrections: hadronic vacuum polarization, finite-size effects, and strong-interaction corrections.

I. INTRODUCTION

We investigate the suitability of deuteronium (the bound system of a deuteron and its antiparticle, the antideuteron) for tests of quantum-electrodynamic interactions involving charged spin-1 particles. Deuteronium constitutes an analogue of protonium, the bound system of proton and antiproton [1, 2], but is distinct in the particle contents, adding a neutron and its antiparticle in the constituent orbiting particles. One of the primary points of interest for deuteronium is that it would allow for the study of higher-order effects in spin-1 bound systems, where the general form of the Breit Hamiltonian for particles of arbitrary spin [3–5] could be subjected to a thorough test, and quantum electrodynamic (QED) vacuum polarization effects could be tested in extreme fields. Specifically, the Coulomb field strength felt by a constituent particle at the (generalized) Bohr radius a_0 of the bound deuteron-antideuteron system (see Table I) is $E_C = 1.7320 \times 10^{18} \frac{\text{V}}{\text{m}}$ and thus exceeds the Schwinger critical field strength $E_{\text{cr}} = 1.3233 \times 10^{18} \frac{\text{V}}{\text{m}}$ (for a recent overview of the latter concept, see Chap. 18 of Ref. [6]).

The derivation of the spin-1 Breit Hamiltonian [5] is a nontrivial exercise, which was completed by the physics community only after combining the results of independent contributions reported over the course of a number of decades. Specifically, after the initial formulation of the relativistic spin-1 wave equation [7, 8], one found a suitable conversion of the equation to a first-order differential equation, to arrive at the Duffin–Kemmer formalism [9, 10], which transforms the Proca equation [7, 8] into a Dirac-like form. One then needs to identify a suitable wave function for the spin-1 system [11, 12], and perform a rather sophisticated Foldy–Wouthuysen transformation in order to derive the spin-1 Hamiltonian, first, for a single particle, and then, for two interacting spin-1 particles [3–5].

It is appropriate to include a few remarks regarding

the availability of antideuterons for the production of the deuteronium bound system. Antideuterons were initially produced in proton-beryllium collisions many years ago (see Refs. [13, 14]). Very promising approaches to antideuteron production at the AD/ELENA facility [15] and at the GBAR beamlines [16] have recently been explored. One possible pathway toward a successful experiment would involve radiative capture of slowed-down antideuteron projectiles in heavy water, or inside an intense atomic beam containing deuterium atoms. The captured antideuteron would cascade down a chain of radiative decays along circular states, lowering the principal quantum number in the transitions [17].

In order to fix ideas and provide a useful reference for the reader, we provide numerical values for a number of physical constants describing properties of the deuteron, and of deuteronium, in Table I. We use natural units with $\hbar = c = \epsilon_0 = 1$ throughout this paper, with two exceptions: one, we restore Système International (SI mksA) units for definiteness in Table I, and two, in the discussion surrounding Eqs. (12), (128), and (130). We adopt a timelike (“West–Coast”) space-time metric, with $g_{00} = +1$, $g_{ij} = -\delta_{ij}$ (where Latin indices are spatial, with $i, j \in \{1, 2, 3\}$).

The scaling the leading radiative and relativistic corrections in deuteronium (with the fine-structure constant α and the deuteron mass m_d) is given in Table II. The leading one-loop vacuum-polarization correction (due to the “Uehling potential” [18]) is of order $\alpha^3 m_d$. This is also the leading correction that leads to the Lamb shifts in deuteronium. The (nonradiative) spin-1–spin-1 Breit interaction enters at order $\alpha^4 m_d$. Among the radiative effects of order $\alpha^4 m_d$, we find both reducible (loop-by-loop) and irreducible [19, 20] two-loop vacuum polarization shifts, and the iterated one-loop electronic vacuum polarization (eVP) effect in second-order perturbation theory. Here, we aim to calculate all corrections to the spectrum up to and including the next-to-leading order, *i.e.*, up to the order $\alpha^4 m_d$, as well as selected corrections

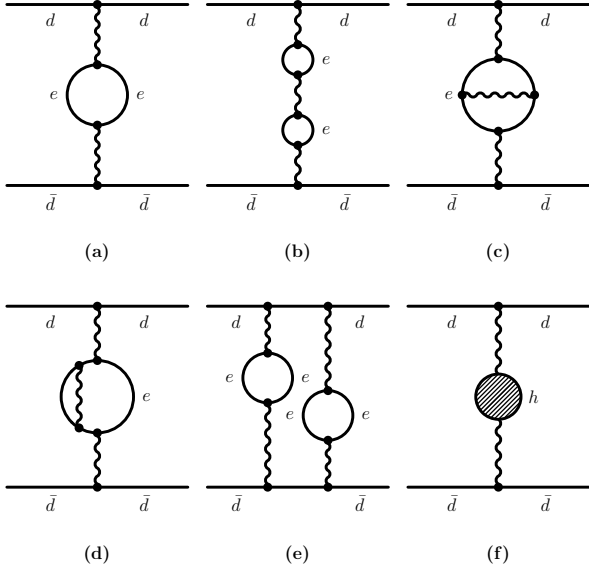


FIG. 1. Feynman diagrams contributing to the leading radiative corrections in deuterium. Light fermions (virtual electrons and positrons) are denoted as “e”, and the hadronic loop is denoted by the letter “h”. Panel (a) represents the leading-order eVP correction, (b) is the loop-by-loop reducible contribution, (c) and (d) are the two independent contributions to the two-loop irreducible correction, (e) represents the second-order perturbation theory contribution of two one-loop potentials, and (f) represents the hadronic vacuum polarization contribution.

connected with the internal structure of the constituent particles. The hadronic vacuum-polarization (VP) effect is included in this list in order to answer a potential question regarding the importance of virtual hadrons in the VP loop, in view of a small Bohr radius for deuterium (Dt). Furthermore, it is indicated to address other internal-structure effects, such as the energy shift due to the deuteron polarizability, as well as finite-size effects and strong-interaction corrections.

Relevant Feynman diagrams for the dominant radiative corrections in deuterium are depicted in Fig. 1; these are due to vacuum-polarization effects. In this work, we put special emphasis on the $2P$, $3P$, $3D$, $4P$, $4D$, and $4F$ states of deuterium, including their spin-dependent (hyper)fine-structure sublevels, because states with nonvanishing orbital angular momenta are much less influenced than S states by strong-interaction effects [2, 21–25]. For S states, these latter effects are large and challenging to analyze [see Ref. [25] and Eq. (132)].

We organize the paper as follows. In Sec. II, we discuss a number of important properties of the deuterium system. The Breit Hamiltonian is treated in Sec. III. Vacuum polarization corrections are discussed in Sec. IV. Effects related to the strong interaction and to the internal structure of the constituent particles are discussed in Sec. V. Finally, the allowed dipole transitions in the sys-

TABLE I. Some useful parameters are given for deuterium (Dt). We use the CODATA recommended values of the fundamental constants [26, 27]. The fine-structure constant is given by $1/\alpha = 137.035\,999\,177(21)$. For the quadrupole moment, we use the result from Ref. [28]. The quadrupole moment of the deuteron is divided by the elementary charge, following commonly adopted conventions (see Refs. [28–30])

Deuteron mass	$m_d c^2 = 1875.612\,945\,00(58)$ MeV
Reduced mass	$m_r c^2 = \frac{1}{2} m_d c^2 = 937.806\,472\,50(29)$ MeV
Dt Bohr radius	$a_0 = \frac{\hbar}{\alpha m_r c} = 28.834\,200\,570(10)$ fm
Dt Hartree	$E_h = \alpha^2 m_r c^2 = 49.939\,464\,871(22)$ keV
Dt Rydberg	$E_0 = \frac{1}{4} \alpha^2 m_d c^2 = 24.969\,732\,435(11)$ keV
NR Spectrum	$E_{\text{NR}} = -\frac{E_0}{n^2} = -\frac{1}{2} \frac{E_h}{n^2} = -\frac{\alpha^2 m_d}{4n^2}$
Dt β Parameter	$\beta_{\text{Dt}} = \frac{m_e}{\alpha m_r} = 0.037\,334\,596\,12(12)$
Deuteron g factor	$g_d = 0.857\,438\,2335(22)$
Scaled g factor	$\tilde{g}_d = (m_d/m_p)g_d = 1.714\,025\,4606(45)$
Deuteron radius	$r_d = 2.12778(27)$ fm
Quad. moment	$Q_d = 0.285\,699(24)$ fm ²

TABLE II. We list the order-of-magnitude (or physical origin) of several energy corrections in deuterium. We evaluate all contributions up to and including those of order $\alpha^4 m_d$, and also some conceptually interesting effects that are linked to the strong interaction and to the internal structure of the constituent particles of Dt.

Effect	Order
One-loop eVP	$\alpha^3 m_d$
Breit Hamiltonian	$\alpha^4 m_d$
Reducible two-loop eVP	$\alpha^4 m_d$
Irreducible two-loop eVP	$\alpha^4 m_d$
Second-order eVP	$\alpha^4 m_d$
Hadronic VP	photon structure
Finite-size	deuteron structure
Deuteron polarizability	deuteron structure
Strong interaction	strong interaction

tem are discussed in Sec. VI. Relevant formulas from the angular-momentum algebra are discussed in Appendix A.

II. BASIC PROPERTIES

In the center-of-mass frame, the nonrelativistic Hamiltonian of deuterium reads as follows,

$$H_{\text{NR}} = \frac{\vec{p}^2}{m_d} - \frac{\alpha}{r}, \quad (1)$$

where \vec{p} is the relative momentum operator in that frame. Convenient quantum numbers for deuterium are the principal quantum number n , the orbital angular momentum quantum number L , the total spin quantum number S describing the magnitude of the total spin $\vec{S} = \vec{S}_+ + \vec{S}_-$ (where \vec{S}_+ and \vec{S}_- are the spin operators for the deuteron and its antiparticle), the total angular momentum quantum number J , and its projection J_z . We denote the states as

$$|n^{2S+1}L_J(J_z)\rangle = |nLSJJ_z\rangle, \quad (2)$$

making use of the spectroscopic notation $n^{2S+1}L_J$ (in which states with $L = 0$ are S states, states with $L = 1$ are P states, etc.). The nonrelativistic wave functions are

$$\psi_{nLSJJ_z}(\vec{r}) = R_{nL}(r) \Xi_{JJ_z}^{LS}(\theta, \varphi), \quad (3)$$

where $R_{nL}(r)$ is a Schrödinger–Coulomb radial eigenfunction of a hydrogenlike ion with nuclear charge number $Z = 1$ and reduced mass $m_r = m_d/2$. Specifically (see, e.g., Chap. 4 of Ref. [6]) one has

$$R_{nL}(r) = \left(\frac{4(n-L-1)!}{a_0^3 n^4 (n+L)!} \right)^{1/2} \rho^L e^{-\rho/2} L_{n-L-1}^{2L+1}(\rho), \quad (4)$$

where $a_0 = 1/(\alpha m_r) = 2/(\alpha m_d)$ is the (generalized) Bohr radius, and $\rho = 2r/(a_0 n)$. The angular part of the wave function for the state $|n^{2S+1}L_J(J_z)\rangle$ is

$$\Xi_{JJ_z}^{LS}(\theta, \varphi) = \sum_{M_L M_S} C_{LM_L; SM_S}^{JJ_z} Y_{LM_L}(\theta, \varphi) \chi_{SM_S}, \quad (5)$$

where χ_{SM_S} is the deuterium total spin state

$$\chi_{SM_S} = \sum_{m_+ m_-} C_{1m_+; 1m_-}^{SM_S} \chi_{m_+}^{(+)} \chi_{m_-}^{(-)}. \quad (6)$$

Here, the $\chi_{m_{\pm}}^{(\pm)}$ are the eigenspinors of the spin operators of the deuteron and the antideuteron. A convenient representation of the spin-1 matrices is $(S_{\pm}^i)^{jk} = -i\epsilon^{ijk}$. These matrices act on the deuteron (+) and antideuteron (−) spinors. They fulfill the relations $(S_{\pm}^z) \chi_{m_{\pm}}^{(\pm)} = m_{\pm} \chi_{m_{\pm}}^{(\pm)}$, where $m_{\pm} \in \{-1, 0, +1\}$. In Eqs. (5) and (6), the Clebsch–Gordan coefficients $C_{j_1 m_1; j_2 m_2}^{JM}$ are used in the notation of Chap. 6 of Ref. [6].

The lowest-order quantum mechanical eigenproblem is solved by

$$H_{\text{NR}} \psi_{nLSJJ_z}(\vec{r}) = E_{\text{NR}} \psi_{nLSJJ_z}(\vec{r}). \quad (7)$$

It gives rise to the nonrelativistic bound-state energy levels which depend only on the principal quantum number n ,

$$E_{\text{NR}} = -\frac{\alpha^2 m_d}{4n^2} = -\frac{E_0}{n^2} \approx -\frac{24969.732 \text{ eV}}{n^2}, \quad (8)$$

where the Dt Rydberg constant E_0 is defined in Table I. One should take into consideration that, strictly speaking, the spin-dependent Breit Hamiltonian (see the following section) is not completely diagonal in the ψ_{nLSJJ_z} basis, so that certain mixings between states with “good” quantum numbers occur in higher orders. Analogous effects occur in hydrogenlike systems, where the effect is otherwise known as the fine-structure hyperfine-structure mixing (for a particularly instructive discussion, in the context of the mixing of the fine and the hyperfine structure for muonic deuterium, see Sec. 6 of Ref. [31]).

The presence of the mixing terms indicates that a careful consideration of the conserved quantum numbers of deuterium is indicated. The total angular momentum J and its z -component J_z are, of course, conserved. Parity and charge parity are conserved in QED. The parity of the antideuteron must be positive, since it is determined by the intrinsic parities of its constituents (both -1) and the parity of the antideuteron quantum state, which is positive since it has the same structure as for the deuteron, being a combination of S and D waves. Then, the parity of a deuterium state is determined by the parities of its constituents (both $+1$) and that of its quantum state $(-1)^L$, for a total parity $P_{\text{Dt}} = (-1)^L$. So the oddness or evenness of L is conserved. Deuterium, being formed of a particle and its antiparticle, can also exist in an eigenstate of charge parity. We determine the charge conjugation quantum number C_{Dt} by considering what happens to a deuterium state when its constituents are interchanged. Since deuterons are bosons, the effect of this interchange is a factor $+1$ for the wave function. A complete interchange involves the exchange of spatial states [with a factor of $(-1)^L$], spin states [factor $(-1)^S$], and charge states (factor C_{Dt}). We find that $+1 = (-1)^L (-1)^S C_{\text{Dt}}$, so that $C_{\text{Dt}} = (-1)^{L+S}$. In all, we have

$$P_{\text{Dt}} = (-1)^L, \quad C_{\text{Dt}} = (-1)^{L+S}, \quad P_{\text{Dt}} C_{\text{Dt}} = (-1)^S. \quad (9)$$

So the oddness or evenness of S is also conserved.

Good states of deuterium are specified by specific values of n , J , and J_z . In addition, they are constructed of states with either even or odd values of L , and either even or odd values of S . One might thus assume that the Breit Hamiltonian could mix states with different values of L provided both states involved in the mixing are even, or, both are odd. However, it is known that the spin-1/2–spin-1/2 Breit Hamiltonian does not mix states with different values of L . Since the spin-1–spin-1 Breit Hamiltonian is built of operators with the same types of spatial dependence, it also does not mix states with different values of L . So, L can be considered to be a good quantum number (to all orders).

The caveat for the total spin is that the Breit Hamiltonian, indeed, mixes spin states, so deuterium states with even spin ($S = 0$ and $S = 2$) can be mixed. Odd-spin states have $S = 1$. It means that, strictly speaking, S is only a good quantum number up to order $\alpha^4 m_d$, when the Breit Hamiltonian starts mixing the spin states. However, the same could be said about the principal quantum number n , since the Uehling potential mixes states with different values of n . We here deal with the Breit Hamiltonian (and the Uehling potential) perturbatively, including contributions of first, second, and (eventually) third-order perturbation theory.

It is instructive to explore the multiplicity and (hyper)fine-structure of the bound states of deuterium for given principal quantum number n and orbital angular momentum L . For S states ($L = 0$), there are three states with $S = J$ equal to 0, 1, or 2. For P states ($L = 1$), when $S = 0$, there is only one possible value of J , namely, $J = 1$. When $S = 1$, J can take any of the three possible values 0, 1, and 2. When $S = 2$, there are also three possible values of $1 \leq J \leq 3$. In all, there are seven P states. In view of the above mentioned symmetry considerations, the only ones that can mix have $S = 0$, $J = 1$ and $S = 2$, $J = 1$. In general, the states that mix have $S = 0$ or $S = 2$ with $L = J$. For D states ($L = 2$), when $S = 0$, the only possible value of J is $J = 2$. When $S = 1$, there are three possible values of J , namely, 1, 2, and 3. When $S = 2$, J can take any value in the set $J \in \{0, 1, 2, 3, 4\}$. In all, there are nine D states. The only ones that can mix have $S = 0$, $J = 2$ and $S = 2$, $J = 2$. For states with $L > 2$, there are also nine states, and the only ones that can mix have $S = 0$, $J = L$ and $S = 2$, $J = L$. The states are explicitly displayed in Table III. We label the states using spectroscopic notation as n^1L_J for $S = 0$, n^3L_J for $S = 1$, and n^5L_J for $S = 2$. The two that mix are n^1L_L and n^5L_L . The states that diagonalize the Breit Hamiltonian are labeled n^-L_L and n^+L_L , where the first has the smaller energy and the second the larger energy. For absolute clarity, we reemphasize that the superscript \pm , in this notation, denotes the superposition of $S = 0$ and $S = 2$ states, and has nothing to do with the parity of the bound state.

The leading corrections to the energies of deuterium are due to the strong interaction and to electron vacuum polarization. The strong interaction shifts are most pronounced in S states, since the ratio of the range of the strong force (≈ 1 fm) to the (generalized) Bohr radius of deuterium ($a_0 \approx 28.8$ fm) is relatively small. Strong interaction shifts are noticeable in P states and negligible for $L \geq 2$. Electron vacuum polarization (the Uehling correction [18]) is by far the leading correction for states with $L \geq 1$, being of order $\alpha^4 m_d$. The corrections due to electron vacuum polarization are spin-independent, depending only on n and L , and can be said to give rise to Lamb shifts such as for $2P-2S$. Spin-dependent shifts commence at order $\alpha^4 m_d$ with the Breit correction, as described in the following section.

III. BREIT HAMILTONIAN

In order to derive the spin-dependent corrections of order $\alpha^4 m_d$ to the spectrum, we generalize the Breit Hamiltonian to the interaction of two spin-1 particles. We use the results communicated in Eq. (3) of Ref. [3] and Eq. (17) of Ref. [4], and Eq. (12.100) of Ref. [6]. An alternative derivation, which starts from the single-particle Hamiltonian for general spin [see Eqs. (1)–(4) of Ref. [5]] has recently been outlined in Ref. [32]. The latter derivation starts from a single-particle spin-1 Hamiltonian, identifies the corresponding Feynman rules of Nonrelativistic Quantum Electrodynamics (NRQED), and leads to the interaction Hamiltonian based on the single-photon interaction kernels identified in Ref. [32].

The Breit Hamiltonian H_{BR} gives corrections of order $\alpha^4 m_d$ to the spectrum. Based on the considerations reported in Refs. [32, 33], we conveniently write the Breit Hamiltonian H_{BR} for an interacting system of two spin-1 particles as follows,

$$H_{\text{BR}} = H_K + H_M + H_{\text{SO}} + H_{\text{FSS}} + H_Q + H_D. \quad (10)$$

This Hamiltonian is the sum of the kinetic term H_K , which describes the relativistic corrections to the kinetic energies of the constituent particles, the magnetic term H_M , which describes the exchange of a transverse photon with convection vertices at each end, the spin-orbit term H_{SO} , the Fermi spin-spin term H_{FSS} , the quadrupole term H_Q which is due to the intrinsic quadrupole moment of the deuteron (and anti-deuteron), and the Dirac delta term H_D , which describes the deuteron finite-size effect, within the Dirac delta approximation (a more thorough treatment is presented in Sec. V B). For convenience, we list them as follows,

$$H_K = -\frac{\vec{p}^4}{4m_d^3}, \quad H_M = -\frac{\alpha}{2m_d^2} p^i \left(\frac{\delta^{ij} + \hat{x}^i \hat{x}^j}{r} \right) p^j, \quad (11a)$$

$$H_{\text{SO}} = \frac{\alpha (2\tilde{g}_d - 1)}{2m_d^2 r^3} (\vec{S}_+ + \vec{S}_-) \cdot \vec{L}, \quad (11b)$$

$$H_{\text{FSS}} = \frac{2\pi\alpha \tilde{g}_d^2}{3m_d^2} \vec{S}_+ \cdot \vec{S}_- \delta^{(3)}(\vec{r}) + \frac{3\alpha \tilde{g}_d^2}{4m_d^2 r^3} (S_+^i S_-^j)^{(2)} (\hat{x}^i \hat{x}^j)^{(2)}, \quad (11c)$$

$$H_Q = -\frac{3\alpha \tilde{Q}_d}{2m_d^2 r^3} [(S_+^i S_+^j)^{(2)} + (S_-^i S_-^j)^{(2)}] (\hat{x}^i \hat{x}^j)^{(2)}, \quad (11d)$$

$$H_D = \frac{4\pi\alpha}{3} \frac{\tilde{r}_d^2}{m_d^2} \delta^{(3)}(\vec{r}). \quad (11e)$$

We recall that Latin superscripts denote spatial components ($i, j = 1, 2, 3$). The unit vector is $\hat{x} = \vec{r}/|\vec{r}|$. Also, $(S_\pm^i S_\pm^j)^{(2)}$ is the quadrupole component of a spin-spin tensor, where the quadrupole component of the tensor product of two vectors \vec{v} and \vec{w} (which do not necessarily commute) is $(v^i w^j)^{(2)} = \frac{1}{2}(v^i w^j + v^j w^i) - \frac{1}{3}\delta^{ij} \vec{v} \cdot \vec{w}$.

Data for the deuteron radius, its electric quadrupole moment, and its g factor (and scaled g factor) can be found in Table I. We note that the dimensionless values of the deuteron radius, r_d , and the deuteron quadrupole moment, Q_d , are (see Refs. [26–28])

$$\tilde{r}_d \equiv m_d r_d = \frac{m_d c}{\hbar} r_d = 20.2248(26) \quad (12)$$

and

$$\tilde{Q}_d = m_d^2 Q_d = \left(\frac{m_d c}{\hbar}\right)^2 Q_d = 25.8120(22), \quad (13)$$

leading to relatively large contributions from these quantities.

The Breit Hamiltonian is derived from the one-photon exchange between the constituent particles of deuterium (no virtual loops) and is the parametrically dominant *nonradiative* correction to the spectrum of deuterium (order $\alpha^4 m_d$). Moreover, the Breit Hamiltonian leads to dominant spin-dependent energy corrections in deuterium. For comparison, we point out that (spin-independent) radiative effects due to vacuum polarization (with a virtual electron-positron loop) are parametrically larger than the Breit corrections and commence at order $\alpha^3 m_d$. These affect the spin-independent structure of deuterium, with dependence only of the quantum numbers n and L , as discussed in Sec. IV A. Higher-order electron vacuum polarization corrections (which are still spin-independent effects) occur at order $\alpha^4 m_d$ and are discussed in Secs. IV C–IV E. Here, we first treat the spin-dependent energy correction E_{BR} which appears at order $\alpha^4 m_d$ due to the Breit Hamiltonian:

$$E_{\text{BR}} = \langle H_{\text{BR}} \rangle = \langle nLSJJ_z | H_{\text{BR}} | nLSJJ_z \rangle. \quad (14)$$

We obtain the corrections coming from the Breit Hamiltonian one term at a time. We start with the kinetic term H_K . In order to evaluate the expectation value of \vec{p}^4 , one observes that the momentum operator acts on wave functions as follows (in our short-hand notation, ψ stands for ψ_{nLSJJ_z}),

$$\vec{p}^2 |\psi\rangle = m_d \left(E_{\text{NR}} + \frac{\alpha}{r} \right) |\psi\rangle, \quad (15)$$

So, one has the relation (we use a further shorthand notation $\langle K \rangle \equiv \langle \psi | K | \psi \rangle$ for any operator K),

$$\begin{aligned} E_K &= \left\langle -\frac{\vec{p}^4}{4m_d^3} \right\rangle = -\frac{1}{4m_d} \left\langle \left(E_{\text{NR}} + \frac{\alpha}{r} \right)^2 \right\rangle \\ &= -\frac{1}{4m_d} \left\langle E_{\text{NR}}^2 + 2E_{\text{NR}} \frac{\alpha}{r} + \left(\frac{\alpha}{r} \right)^2 \right\rangle \\ &= \alpha^4 m_d \left\{ \frac{3}{64n^4} - \frac{1}{8n^3(2L+1)} \right\}. \end{aligned} \quad (16)$$

We have used the following matrix elements from

Eq. (4.346) of Ref. [6],

$$\left\langle \frac{1}{r} \right\rangle = \frac{\alpha m_d}{2n^2}, \quad (17a)$$

$$\left\langle \frac{1}{r^2} \right\rangle = \frac{\alpha^2 m_d^2}{2n^3(2L+1)}. \quad (17b)$$

The magnetic term H_M is conveniently evaluated by using the following identity,

$$\begin{aligned} H_M &= -\frac{\alpha}{2m_d^2} p^i \left(\frac{\delta^{ij}}{r} + \frac{r^i r^j}{r^3} \right) p^j \\ &= -\frac{\alpha}{2m_d^2 r} \left(\vec{p}^2 + \frac{1}{r^2} [\vec{r} \cdot (\vec{r} \cdot \vec{p}) \vec{p}] \right). \end{aligned} \quad (18)$$

This relation is consistent with Eq. (84.1) of Ref. [34]. Use of Eq. (15) leads to the appearance of matrix elements proportional to $\langle 1/r^3 \rangle$, which can be evaluated using Eq. (4.346) of Ref. [6],

$$\left\langle \frac{1}{r^3} \right\rangle = \frac{\alpha^3 m_d^3}{4n^3 L(L+1)(2L+1)}, \quad (19)$$

which is divergent for S states with $L = 0$. However, a closer inspection reveals that the matrix element $E_M = \langle H_M \rangle$ is convergent for S states, and one obtains the general formula

$$E_M = \frac{\alpha^4 m_d}{8n^4} + \frac{\alpha^4 m_d}{8n^3} \delta_{L0} - \frac{3\alpha^4 m_d}{8n^3(2L+1)}. \quad (20)$$

The next term is the spin-orbit term H_{SO} . One writes the total spin operator (sum for both particles) as $\vec{S} = \vec{S}_+ + \vec{S}_-$, and obtains

$$E_{\text{SO}} = \frac{\alpha(2\tilde{g}_d - 1)}{2m_d^2} \langle \vec{L} \cdot \vec{S} \rangle \left\langle \frac{1}{r^3} \right\rangle. \quad (21)$$

With use of the definition

$$B_{LSJ} = \frac{1}{2} [J(J+1) - L(L+1) - S(S+1)] \quad (22)$$

one has

$$\langle \vec{L} \cdot \vec{S} \rangle = B_{LSJ}. \quad (23)$$

So,

$$E_{\text{SO}} = \frac{\alpha(2\tilde{g}_d - 1)}{2m_d^2} B_{LSJ} \left\langle \frac{1}{r^3} \right\rangle. \quad (24)$$

The remaining matrix element $\langle 1/r^3 \rangle$ is evaluated using Eq. (19). The energy shift E_{SO} vanishes for S states by spherical symmetry (despite the apparent $1/L$ singularity when $L = 0$).

The scalar part of the Fermi-spin-spin energy correction,

$$E_{\text{FSS},1} = \frac{2\pi\alpha\tilde{g}_d^2}{3m_d^2} \langle \vec{S}_+ \cdot \vec{S}_- \delta^{(3)}(\vec{r}) \rangle, \quad (25)$$

is relatively easy to evaluate. First, one realizes that the expectation value of the Dirac delta is $\langle \delta^{(3)}(\vec{r}) \rangle = \frac{(\alpha m_d)^3}{8\pi n^3} \delta_{L0}$. With the help of the identity

$$\langle \vec{S}_+ \cdot \vec{S}_- \rangle = \frac{1}{2} [S(S+1) - 4], \quad (26)$$

one obtains the result

$$E_{\text{FSS},1} = \tilde{g}_d^2 \frac{\alpha^4 m_d}{24 n^3} [S(S+1) - 4] \delta_{L0}. \quad (27)$$

For the tensor part of the Fermi spin-spin term,

$$H_{\text{FSS},2} = \frac{3\alpha \tilde{g}_d^2}{4m_d^2 r^3} (S_+^i S_-^j)^{(2)} (\hat{x}^i \hat{x}^j)^{(2)} \quad (28)$$

and the quadrupole term

$$H_Q = -\frac{3\alpha \tilde{Q}_d}{2m_d^2 r^3} [(S_+^i S_+^j)^{(2)} + (S_-^i S_-^j)^{(2)}] (\hat{x}^i \hat{x}^j)^{(2)}, \quad (29)$$

one needs to carry out some more angular algebra. We need to evaluate matrix elements involving different values of the total spin instead of simply expectation values, since these terms are non-diagonal in the spin variable. We thus consider an “almost diagonal” matrix element $\langle f(r)M \rangle_{nLS'SJ} \equiv \langle nLS'JJ_z | f(r)M | nLSJJ_z \rangle$, where all quantum numbers of the bra and ket states are equal except, possibly, for different S and S' . The operator $f(r)$ is supposed to have only a radial dependence, and M is assumed to depend only on the elements of the unit vector \hat{x} , and on the spin variables. With reference to the radial component of the wave function [see Eq. (3)], we can first separate out the radial dependence using

$$\langle f(r)M \rangle_{nLS'SJ} = \int dr r^2 [R_{nL}(r)]^2 f(r) \langle M \rangle_{LS'SJ} \quad (30)$$

when M is independent of the radial variable and

$$\langle X \rangle_{LS'SJ} \equiv \langle LS'J | X | LSJ \rangle \quad (31)$$

for any operator X . Employing relations derived in Appendix A, which are based on angular reduction, one derives the following angular matrix elements:

$$\begin{aligned} D_{LS'SJ} &\equiv \left\langle [(S_+^i S_+^j)^{(2)} + (S_-^i S_-^j)^{(2)}] (\hat{x}^i \hat{x}^j)^{(2)} \right\rangle_{LS'SJ} \\ &= (-1)^{J+S'} \left[(-1)^S + (-1)^{S'} \right] \sqrt{\frac{10}{3}} (2L+1) \\ &\times \Pi_{S'S} \begin{Bmatrix} J & S' & L \\ 2 & L & S \end{Bmatrix} \begin{pmatrix} L & 2 & L \\ 0 & 0 & 0 \end{pmatrix} \begin{Bmatrix} S & S' & 2 \\ 1 & 1 & 1 \end{Bmatrix}, \quad (32) \end{aligned}$$

and

$$\begin{aligned} C_{LS'SJ} &\equiv \left\langle (S_+^i S_-^j)^{(2)} (\hat{x}^i \hat{x}^j)^{(2)} \right\rangle_{LS'SJ} \\ &= (-1)^{(S+S')/2} \frac{1}{2} (1 + \delta_{S'S}) D_{LS'SJ}, \quad (33) \end{aligned}$$

where $\Pi_{ab\dots} \equiv \sqrt{(2a+1)(2b+1)\dots}$. Standard notation is used for the Wigner $3j$ and $6j$ symbols (see Chap. 6 of Ref. [6]). One thus obtains the result

$$\begin{aligned} &\langle H_{\text{FSS},2} + H_Q \rangle_{nLS'SJ} \\ &= \frac{3\alpha}{4m_d^2} \{ \tilde{g}_d^2 C_{LS'SJ} - 2\tilde{Q}_d D_{LS'SJ} \} \left\langle \frac{1}{r^3} \right\rangle \\ &= \frac{m_d \alpha^4}{n^3} \times \frac{3(\tilde{g}_d^2 C_{LS'SJ} - 2\tilde{Q}_d D_{LS'SJ})}{16L(L+1)(2L+1)}. \quad (34) \end{aligned}$$

Both $C_{LS'SJ}$ and $D_{LS'SJ}$ vanish when $L = 0$ by spherical symmetry, and this zero in the numerator takes precedence over the apparent singularity caused by L in the denominator.

Finally, for the Dirac delta contribution, one has

$$E_D = \frac{4\pi\alpha}{3m_d^2} \tilde{r}_d^2 \langle \delta^{(3)}(\vec{r}) \rangle = \frac{\alpha^4 m_d}{6n^3} \tilde{r}_d^2 \delta_{L0}. \quad (35)$$

Let us fix the quantum number n , L , J , and J_z , and consider the matrix elements of the Breit Hamiltonian in the basis of the total spin quantum numbers S and S' , which takes values equal to 0, 1 and 2. In the basis of the S and S' quantum numbers, one thus obtains a three-by-three matrix. According to the above mentioned symmetry considerations, the resulting matrix is diagonal except for the case $L = J$, where one encounters off-diagonal elements for $S' = 2$, $S = 0$ and $S' = 0$, $S = 2$. Summing up the results given in Eqs. (16), (20), (24), (27), (34) and (35), one obtains

$$\begin{aligned} \langle H_{\text{BR}} \rangle_{nLS'SJJ_z} &= \langle nLS'JJ_z | H_{\text{BR}} | nLSJJ_z \rangle \\ &\equiv \alpha^4 m_d M_{S'S}^{nLJ}. \quad (36) \end{aligned}$$

The results are, of course, independent of J_z . The explicit expression for $M_{S'S}^{nLJ}$ is

$$\begin{aligned} M_{S'S}^{nLJ} &= \left(\frac{11}{64n^4} - \frac{1}{2n^3(2L+1)} \right) \delta_{S'S} \\ &+ \frac{\delta_{L0}}{8n^3} \left(1 + \frac{4}{3} \tilde{r}_d^2 + \frac{\tilde{g}_d^2}{3} [S(S+1) - 4] \right) \delta_{S'S} \\ &+ \frac{(2\tilde{g}_d - 1) B_{LSJ}}{8n^3 L(L+1)(2L+1)} \delta_{S'S} \\ &+ \frac{3(\tilde{g}_d^2 C_{LS'SJ} - 2\tilde{Q}_d D_{LS'SJ})}{16n^3 L(L+1)(2L+1)}. \quad (37) \end{aligned}$$

The angular structures B_{LSJ} , $C_{LS'SJ}$, and $D_{LS'SJ}$ are defined in Eqs. (22), (33) and (32).

For most values of L and J , the $M_{S'S}^{nLJ}$ matrices are diagonal, but when $L = J$, the submatrix spanned by the spin quantum numbers $S', S \in \{0, 2\}$ is not diagonal. For example, for $n = 2$, $L = J = 1$, the $M_{S'S}^{2,1,1}$ matrix is a (3×3) -matrix in the basis with $S', S \in \{0, 1, 2\}$ and reads as follows,

$$M^{2,1,1} = \begin{pmatrix} -0.01009 & 0 & 0.12367 \\ 0 & 0.05463 & 0 \\ 0.12367 & 0 & 0.05969 \end{pmatrix}. \quad (38)$$

The element in the center of the matrix corresponds to the case $S = S' = 1$ and does not couple to the states with other values of S . The eigenvalues of the matrix are -0.10369 , 0.05463 , and 0.15329 . The states n^-L_L and n^+L_L are constructed using the $S = 0$ and $S = 2$ states n^1L_L and n^5L_L to diagonalize the Breit Hamiltonian, with n^-L_L (n^+L_L) being associated with the lower (higher) energy eigenvalue. Numerical results for Breit energies are presented in Table III.

IV. VACUUM POLARIZATION

A. One-Loop Electronic VP

In momentum space, the Coulomb potential takes the form $V(\vec{k}) = -4\pi\alpha/\vec{k}^2$, where we set the nuclear charge number $Z = 1$. The one-loop correction to the Coulomb potential, pictured in Fig. 1(a), is given by the replacement

$$-\frac{4\pi\alpha}{\vec{k}^2} \rightarrow -\frac{4\pi\alpha}{\vec{k}^2} \left[-\Pi_{\text{R}}^{(1)}(-\vec{k}^2) \right], \quad (39)$$

where $\Pi_{\text{R}}^{(1)}(-\vec{k}^2)$ is the renormalized one-loop vacuum polarization function in the conventions of Ref. [20], evaluated for space-like momentum transfer $k^2 = -\vec{k}^2$. After using a dispersion relation, one may express the (electronic) vacuum polarization potential as

$$V_{\text{eVP}}^{(1)}(r) = -\frac{\alpha}{\pi} \frac{2}{r} \int_{2m_e}^{\infty} dq \frac{e^{-qr}}{q} \text{Im} \left[\Pi_{\text{R}}^{(1)}(q^2 + i\epsilon) \right]. \quad (40)$$

With the substitution [35]

$$v = \sqrt{1 - \frac{4m_e^2}{q^2}}, \quad q = \frac{2m_e}{\sqrt{1 - v^2}}, \quad (41)$$

one may thus express the one-loop Uehling potential as follows (see Ref. [18]),

$$V_{\text{eVP}}^{(1)}(r) = \frac{\alpha}{\pi} \int_0^1 dv f_1(v) e^{-\lambda_e(v)r} \left(-\frac{\alpha}{r} \right), \quad (42)$$

where $\lambda_e(v) \equiv 2m_e/\sqrt{1 - v^2}$ and we define the one-loop spectral function as

$$f_1(v) = \frac{2v}{1 - v^2} \frac{\text{Im} \Pi_{\text{R}}^{(1)}(v)}{\alpha} = \frac{v^2(1 - v^2/3)}{1 - v^2}. \quad (43)$$

The energy shift due to this potential is

$$E_{\text{eVP}}^{(1)} = \langle V_{\text{eVP}}^{(1)} \rangle = \int dr r^2 [R_{nL}(r)]^2 V_{\text{eVP}}^{(1)}(r). \quad (44)$$

There is no dependence on the spin. Using the non-relativistic wave functions given in Eq. (3), one finds that

$$E_{\text{eVP}}^{(1)} = \left(\frac{\alpha}{\pi} \right) E_0 C(n, L), \quad (45)$$

TABLE III. Relativistic corrections to the deuterium energy levels at order $\alpha^4 m_d$ coming from the Breit Hamiltonian. Results are given for $n^{2S+1}L_J$ levels with $n \in \{2, 3, 4\}$, $L \geq 1$, and all possible combinations of S and J . The uncertainties quoted here are due completely to the uncertainty in Q_d , since r_d , which also has a relatively large uncertainty, only enters for S states, and the remaining quantities involved have negligible uncertainties. The $n^\pm L_L$ states are linear combinations of n^1L_L and n^5L_L found by diagonalization of the Breit Hamiltonian [see the discussion near the end of Sec. II and Eq. (38)].

$2^{2S+1}P_J$	E_{BR} (meV)	$3^{2S+1}P_J$	E_{BR} (meV)
2^-P_1	-551.52(6)	3^-P_1	-169.06(2)
2^+P_1	815.32(6)	3^+P_1	235.93(2)
2^3P_0	-876.66(6)	3^3P_0	-265.39(2)
2^3P_1	290.56(3)	3^3P_1	80.449(9)
2^3P_2	-95.614(6)	3^3P_2	-33.973(2)
2^5P_2	-559.34(4)	3^5P_2	-171.373(13)
2^5P_3	148.457(12)	3^5P_3	38.344(4)
$3^{2S+1}D_J$	E_{BR} (meV)	$4^{2S+1}P_J$	E_{BR} (meV)
3^-D_2	-49.419(3)	4^-P_1	-72.511(7)
3^+D_2	18.051(3)	4^+P_1	98.344(8)
3^3D_1	-36.784(2)	4^3P_0	-113.153(8)
3^3D_2	11.986(2)	4^3P_1	32.749(4)
3^3D_3	-10.8249(5)	4^3P_2	-15.5226(8)
3^5D_0	19.590(4)	4^5P_2	-73.488(6)
3^5D_1	1.603(2)	4^5P_3	14.9862(15)
3^5D_3	-31.248(2)		
3^5D_4	10.9760(10)		
$4^{2S+1}D_J$	E_{BR} (meV)	$4^{2S+1}F_J$	E_{BR} (meV)
4^-D_2	-22.0388(12)	4^-F_3	-8.9600(4)
4^+D_2	6.4249(11)	4^+F_3	1.1213(4)
4^3D_1	-16.7084(8)	4^3F_2	-6.2652(2)
4^3D_2	3.8662(8)	4^3F_3	0.7084(3)
4^3D_3	-5.7571(2)	4^3F_4	-2.58892(9)
4^5D_0	7.0744(15)	4^5F_1	0.0494(5)
4^5D_1	-0.5141(8)	4^5F_2	-2.96259(11)
4^5D_3	-14.3730(9)	4^5F_4	-5.0753(3)
4^5D_4	3.4402(5)	4^5F_5	1.4435(2)

where E_0 is the deuteronium Rydberg (as given in Table I) and the dimensionless coefficient $C(n, L)$ is

$$C(n, L) = \left(-\frac{2(n-L-1)!}{n^2(n+L)!} \right) \int_0^1 dv f_1(v) \times \int_0^\infty d\rho \rho^{2L+1} e^{-\rho} [L_{n-L-1}^{2L+1}(\rho)]^2 e^{-n\beta_{\text{Dt}} \rho / \sqrt{1-v^2}}, \quad (46)$$

and $\beta_{\text{Dt}} = m_e/(\alpha m_r)$ has been given in Table I. For given n and L , the ρ integral can easily be performed analytically, and the v integral can be performed numerically. (We should note that, for individual states, fully analytic results exist [20, 36], but the numerical integration proceeds without problems [37] with the built-in numerical integration routines of modern computer algebra systems.) One notes that the potentially singular terms in $1/(1-v^2)$ cancel naturally after the integration over ρ . The numerical results are shown in Table IV. As examples, the $1S$ energy correction is mainly determined by electron vacuum polarization:

$$E_{\text{eVP}}^{(1)}(1S) = -125.203\,42\,\text{eV}, \quad (47)$$

and the $n = 3$ Lamb shift due to electron vacuum polarization is

$$E_{\text{eVP}}^{(1)}(3P-3S) = 1.89842\,\text{eV} \rightarrow 653.09\,\text{nm}. \quad (48)$$

The one-loop eVP shift is by far the dominant radiative correction in heavy bound systems [36, 38–45].

B. One-Loop Muonic VP

In muonic bound systems, one can approximate the muonic vacuum polarization potential by a Dirac delta potential [39, 46], because the mass scale of the bound particle (the muon) is equal to the mass of the virtual muon in the vacuum polarization loop. It means that, for muonic bound systems and muonic vacuum polarization, the effective β parameter in Eq. (46) is large, approximately equal to $1/\alpha$. Hence, muonic vacuum polarization effects are drastically suppressed for bound systems where the orbiting particle is a muon, and are in fact of order $\alpha^5 m_r$ for S states and of higher order than $\alpha^5 m_r$ for non- S states. It is a characteristic of the deuteronium bound system that muonic vacuum polarization even makes a substantial contribution to the bound-state energy of non- S states, because the β parameter for muonic vacuum polarization in deuteronium,

$$\beta_{\text{Dt}}^\mu = \frac{m_\mu}{\alpha m_r} \approx 15.4 \ll 137.0 \approx 1/\alpha, \quad (49)$$

is much smaller than the inverse of the fine-structure constant. For muonic vacuum polarization, one replaces, in Eq. (46),

$$\beta_{\text{Dt}} \rightarrow \beta_{\text{Dt}}^\mu. \quad (50)$$

The muonic vacuum polarization potential is

$$V_{\mu\text{VP}}^{(1)}(r) = \frac{\alpha}{\pi} \int_0^1 dv f_1(v) e^{-\lambda_\mu(v)r} \left(-\frac{\alpha}{r} \right), \quad (51)$$

where

$$\lambda_\mu(v) = \frac{2m_\mu}{\sqrt{1-v^2}}, \quad (52)$$

and the energy shift is

$$E_{\mu\text{VP}}^{(1)} = \langle V_{\mu\text{VP}}^{(1)}(r) \rangle. \quad (53)$$

Results for the one-loop muonic energy $E_{\mu\text{VP}}^{(1)}$ are summarized in Table IV. While results are strongly suppressed for states with orbital angular momentum $L \geq 2$, substantial energy shifts are encountered for S and P states.

C. Reducible Two-Loop Correction

In momentum space, the reducible two-loop correction [see Fig. 1(b)], the loop-after-loop correction, can be described by the replacement of the Coulomb potential according to [cf. Eq. (39)]

$$-\frac{4\pi\alpha}{\vec{k}^2} \rightarrow -\frac{4\pi\alpha}{\vec{k}^2} [\Pi_{\text{R}}^{(1)}(-\vec{k}^2)]^2. \quad (54)$$

Hence, we can use the formalism used for the one-loop correction, but with the one-loop polarization function $\Pi_{\text{R}}^{(1)}$ squared,

$$V^{(2\text{R})}(r) = -\frac{\alpha}{\pi} \frac{2}{r} \int_{2m_e}^\infty dq \frac{e^{-qr}}{q} \text{Im} \left[-\left(\Pi_{\text{R}}^{(1)}(q^2 + i\epsilon) \right)^2 \right]. \quad (55)$$

One may use the identity

$$\text{Im} \left[\left(\Pi_{\text{R}}^{(1)}(q^2 + i\epsilon) \right)^2 \right] = 2 \text{Re} [\Pi_{\text{R}}^{(1)}(q^2)] \text{Im} [\Pi_{\text{R}}^{(1)}(q^2 + i\epsilon)] \quad (56)$$

above threshold $q^2 > 4m_e^2$, in order to simplify the expression. We recall from Ref. [20] that

$$\Pi_{\text{R}}^{(1)}(q^2 + i\epsilon) = \frac{\alpha}{\pi} \left[\frac{1}{9} (8 - 3\tilde{v}^2) - \frac{1}{6} \tilde{v} (\tilde{v}^2 - 3) \ln \left(\frac{\tilde{v} - 1}{\tilde{v} + 1} \right) \right]. \quad (57)$$

where

$$\tilde{v} = \sqrt{1 - \frac{4m_e^2}{q^2 + i\epsilon}}. \quad (58)$$

On the cut ($q^2 > 4m_e^2$), \tilde{v} becomes $v + i\epsilon$, where $v = \sqrt{1 - 4m_e^2/q^2}$ satisfies $0 < v < 1$. The logarithm in Eq. (57) transforms as follows

$$\ln \left(\frac{\tilde{v} - 1}{\tilde{v} + 1} \right) = \ln \left(\frac{1 - v}{1 + v} \right) + i\pi. \quad (59)$$

TABLE IV. Contributions to the Lamb shift in deuterium in units of meV. The second column shows the energy shift due to electron vacuum polarization (the Uehling shift). The third column gives the contribution of muon vacuum polarization, the fourth of loop-by-loop reducible electron vacuum polarization, the fifth of two-loop irreducible electron vacuum polarization, and the sixth of the second-order perturbation theory with two electron vacuum polarization potentials. The “total VP” column contains the sum of the previous four, in meV. The final three columns give the finite size correction, the correction due to scalar polarizability, and the strong interaction contribution.

Level nL	$E_{\text{eVP}}^{(1)}$ (meV)	$E_{\mu\text{VP}}^{(1)}$ (meV)	$E_{\text{VP}}^{(2\text{R})}$ (meV)	$E_{\text{VP}}^{(2\text{I})}$ (meV)	$E_{\text{VP}}^{(1+1)}$ (meV)	total VP (meV)	E_{FS} (meV)	E_{PS} (meV)	E_{S} (meV)
2P	-9692.68328	-0.00331	-10.46921	-60.10373	-16.57279	-87.14904	5.83	-54.94(12)	130(130)
3P	-2517.83207	-0.00116	-2.86332	-15.78409	-2.95501	-21.60358	2.05	-18.09(4)	46(46)
3D	-1274.84951	-0.00000	+0.08013	-10.58606	-1.18435	-11.69028	0.00003	-0.7235(15)	0.00051(51)
4P	-1004.06887	-0.00052	-1.22505	-6.16306	-0.92152	-8.31015	0.911	-7.898(16)	20(20)
4D	-488.20600	-0.00000	-0.05248	-3.88547	-0.35325	-4.29120	0.00002	-0.3434(7)	0.00031(31)
4F	-189.07576	-0.00000	+0.15319	-1.97191	-0.08324	-1.90196	0.00000	-0.04906(10)	0.00000

So, on the cut, one has

$$\text{Im}[\Pi_{\text{R}}^{(1)}(q^2 + i\epsilon)] = \frac{\alpha v}{6} (3 - v^2). \quad (60)$$

The real part, for $q^2 > 4m_e^2$, is

$$\text{Re}[\Pi_{\text{R}}^{(1)}(q^2 + i\epsilon)] = \frac{\alpha}{\pi} \left[\frac{8 - 3v^2}{9} - \frac{v^3 - 3v}{6} \ln \left(\frac{1 - v}{1 + v} \right) \right]. \quad (61)$$

The one-loop spectral function from Eq. (43) is

$$f_1(v) = \frac{2v}{1 - v^2} \frac{\text{Im} \Pi_{\text{R}}^{(1)}(v)}{\alpha}. \quad (62)$$

For the two-loop reducible diagram, we can define a corresponding spectral function

$$\begin{aligned} f_{2\text{R}}(v) &= \frac{2v}{1 - v^2} \frac{\pi}{\alpha^2} \text{Im} \left[- \left(\Pi_{\text{R}}^{(1)}(q^2 + i\epsilon) \right)^2 \right] \\ &= -2f_1(v) \left[\frac{8 - 3v^2}{9} - \frac{v(v^2 - 3)}{6} \ln \left(\frac{1 - v}{1 + v} \right) \right]. \end{aligned} \quad (63)$$

(64)

The two-loop reducible potential thus is

$$V_{\text{VP}}^{(2\text{R})}(r) = \left(\frac{\alpha}{\pi} \right)^2 \int_0^1 dv f_{2\text{R}}(v) e^{-\lambda_e(v)r} \left(-\frac{\alpha}{r} \right), \quad (65)$$

and the remaining evaluation of

$$E_{\text{VP}}^{(2\text{R})} = \left\langle V_{\text{VP}}^{(2\text{R})}(r) \right\rangle \quad (66)$$

proceeds as outlined in Sec. IV A. Results for $E_{\text{VP}}^{(2\text{R})}$ are given in Table IV.

D. Irreducible Two-Loop Correction

The two-loop irreducible vacuum polarization function [see Figs. 1(c) and (d)] was initially calculated by Kallen

and Sabry [19] and by Schwinger [47]. A convenient form was recently obtained in Ref. [20] for the imaginary part of the two-loop irreducible vacuum polarization function above threshold ($q^2 > 4m_e^2$):

$$\begin{aligned} \frac{\pi}{\alpha^2} \text{Im}[\Pi_{\text{R}}^{(2\text{I})}(q^2 + i\epsilon)] &= \frac{v(5 - 3v^2)}{8} \\ &+ \frac{1}{48} (7v^4 - 22v^2 - 33) \ln(-x) \\ &+ \frac{v(3 - v^2)}{6} \left[2\Phi_1(x) + 3 \ln(-x) \right] \\ &+ \frac{(v^2 - 3)(v^2 + 1)}{6} \left[\Phi_1(x) \ln(-x) - 2\Phi_2(x) \right] \end{aligned} \quad (67)$$

where $x \equiv (v - 1)/(v + 1)$ and $\Phi_n(x) = \text{Li}_n(x) + 2\text{Li}_n(-x)$ with $\text{Li}_1(x) \equiv -\ln(1 - x)$. One defines, in analogy with Eq. (62),

$$f_{2\text{I}}(v) = \frac{2v}{1 - v^2} \frac{\pi}{\alpha^2} \text{Im}[\Pi_{\text{R}}^{(2\text{I})}(v)]. \quad (68)$$

The irreducible two-loop potential is thus

$$V_{\text{VP}}^{(2\text{I})}(r) = \left(\frac{\alpha}{\pi} \right)^2 \int_0^1 dv f_{2\text{I}}(v) e^{-\lambda_e(v)r} \left(-\frac{\alpha}{r} \right). \quad (69)$$

The remaining evaluation of

$$E_{\text{VP}}^{(2\text{I})} = \langle V_{\text{VP}}^{(2\text{I})}(r) \rangle \quad (70)$$

proceeds in full analogy to the one-loop and two-loop reducible energy shifts. Results are shown in Table IV.

E. Second-Order Vacuum-Polarization

The vacuum-polarization correction also makes a contribution in second-order perturbation theory [see Fig. 1(e)],

$$E_{\text{VP}}^{(1+1)} = \langle V_{\text{VP}}^{(1)} \hat{G}_{nL} V_{\text{VP}}^{(1)} \rangle, \quad (71)$$

where \hat{G}_{nL} is the reduced Green function for the reference state. (The reduced Green function has the contribution of the reference state subtracted out, after which the limit as the energy becomes that of the reference state is taken.) Convenient coordinate-space forms for these reduced Green functions have been given in Ref. [48] in terms of the radial reduced Green function \hat{g}_{nL} , where

$$\hat{G}_{nL}(\vec{r}_1, \vec{r}_2) = \hat{g}_{nL}(r_1, r_2) \sum_m Y_{Lm}(\theta_1, \phi_1) Y_{Lm}^*(\theta_2, \phi_2). \quad (72)$$

where \hat{g}_{nL} is radial component, and L is the orbital angular momentum of the reference state. We should remark that a couple of corrections are necessary in Ref. [48]: $\ln(x)$ in the first line of (2.14) should be $\ln(x_>)$, and e^x and x^k in the last line of Eq. (2.18) of Ref. [48] should be $e^{x_<}$ and $(x_<)^k$ [49]. We also must multiply \hat{g}_{nL} by αm_r^2 to convert from the atomic units used in Ref. [48] to our natural units. The \hat{g}_{nL} radial reduced Green functions for $n \in \{1, 2, 3\}$ were also given explicitly in Ref. [50], and a general expression in terms of Whittaker functions for the unreduced radial Green function g_{nL} is given in Sec. 4.3.2 of [6]. Upon making use of the orthonormality of spherical harmonics, the energy shift becomes

$$E_{\text{VP}}^{(1+1)} = \int dr_1 dr_2 r_1^2 r_2^2 R_{nL}(r_1) V_{\text{eVP}}^{(1)}(r_1) \hat{g}_{nL}(r_1, r_2) \times V_{\text{eVP}}^{(1)}(r_2) R_{nL}(r_2). \quad (73)$$

It can be written in terms of a dimensionless integral as

$$E_{\text{VP}}^{(1+1)} = \left(\frac{\alpha}{\pi}\right)^2 E_0 D(n, L), \quad (74)$$

where

$$D(n, L) = \frac{4}{n} \left(\frac{p!}{q!}\right)^2 \int_0^1 du f_1(u) \int_0^1 dv f_1(v) \times \int_{\rho_2 < \rho_1} d\rho_1 d\rho_2 (\rho_1 \rho_2)^s e^{-[\rho_1 \omega(u) + \rho_2 \omega(v)]} \times L_p^s(\rho_1) h_{nL}(\rho_1, \rho_2) L_p^s(\rho_2) \quad (75)$$

where $p \equiv n - L - 1$, $q \equiv n + L$, $s \equiv 2L + 1$,

$$\omega(v) \equiv 1 + n\beta_{\text{Dt}}/\sqrt{1-v^2}, \quad (76)$$

and

$$\hat{g}_{nL}(r_1, r_2) = (\alpha m_r^2) \frac{4p!}{nq!} (\rho_1 \rho_2)^L e^{-\frac{\rho_1 + \rho_2}{2}} h_{nL}(\rho_1, \rho_2) \quad (77)$$

with the usual relations [see Eq. (4)] between the radial variables r and their dimensionless partners ρ . The reduced radial Green functions $h_{nL}(\rho_1, \rho_2)$ were obtained from Eq. (2.18) of [48], being specifically the part of that equation inside the curly bracket (with the corrections mentioned earlier). For example,

$$h_{10}(\rho_1, \rho_2) = \left\{ -\frac{7}{2} + 2\gamma_E - \frac{1}{\rho_1} - \frac{1}{\rho_2} + \frac{\rho_1}{2} + \frac{\rho_2}{2} + \frac{e^{\rho_2}}{\rho_2} - \text{Ei}(\rho_2) + \ln(\rho_1 \rho_2) \right\}, \quad (78)$$

which holds when $\rho_2 < \rho_1$. The radial integral over ρ_2 can be performed analytically and the integration over ρ_1 , v and w proceeds numerically [37]. Results for $E_{\text{VP}}^{(1+1)}$ are given in Table IV.

V. INTERNAL-STRUCTURE EFFECTS

A. Hadronic VP: Calculation

Even though hadronic VP [see Fig. 1(f)] constitutes a numerically small energy correction, it is an extremely interesting effect to study as it pertains to the internal hadronic structure of the virtual photons exchanged between the constituent particles of deuteronium. Our approach, as outlined below, is inspired by Refs. [40, 41], where hadronic VP effects were studied for true muonium (alternatively referred to as dimuonium, the $\mu^+\mu^-$ bound system). The strategy will be as follows. (i) The dominant contribution to hadronic vacuum polarization comes from the pion form factor, which has been given in a particularly useful parameterization in Ref. [51]. (ii) The ω and ϕ meson contributions are taken into account in the pole approximation. (iii) Finally, the high-energy background above 1 GeV is estimated by taking into account the R ratio of the relevant cross sections of virtual photons into hadronic versus light fermionic particles, in the high-energy region.

First, we deal with the pionic contribution. The hadronic VP insertion is described by the following replacement of the momentum space Coulomb potential, [see Eq. (2.1) of Ref. [52] and Eq. (1) of Ref. [40]],

$$-\frac{4\pi\alpha}{\vec{k}^2} \rightarrow -\frac{\alpha}{\pi} \int_{s_0}^{\infty} ds \rho_{\text{had}}(s) \frac{4\pi\alpha}{\vec{k}^2 + s}, \quad (79)$$

where $\rho_{\text{had}}(s)$ is the hadronic contribution to the vacuum polarization spectral function. We assume that the spectral function $\rho_{\text{had}}(s)$ has a sufficiently complicated form so that analytic evaluations are impossible. After a transformation to coordinate space, the hadronic vacuum polarization potential takes the form

$$V_{\text{had}}(r) = \frac{\alpha}{\pi} \left(-\frac{\alpha}{r}\right) \int_{s_0}^{\infty} ds \rho_{\text{had}}(s) e^{-\sqrt{s}r}. \quad (80)$$

For the pion insertion, one obtains

$$V_{\pi}(r) = \frac{\alpha}{\pi} \left(-\frac{\alpha}{r}\right) \int_{s_0}^{\infty} ds \rho_{\pi}(s) e^{-\sqrt{s}r}, \quad (81)$$

with $s_0 = (2m_{\pi})^2$. We are inspired by the approach outlined in Ref. [52]. The spectral function is of the form

$$\rho_{\pi}(s) = \frac{(s - 4m_{\pi}^2)^{3/2}}{12s^{5/2}} |F_{\pi}(s)|^2, \quad (82)$$

where the pionic form factor is used in the form given by Gounaris and Sakurai [51]:

$$F_{\pi}(s) = \frac{N}{D_1 + D_2 - iD_3} \approx \frac{N}{D_1 - iD_3}. \quad (83)$$

According to Eq. (11) of Ref. [51], the pion form factor can be approximated in terms of the quantities N , D_1 , D_2 and D_3 , as follows,

$$N = m_\rho^2 + d m_\rho \Gamma_\rho = m_\rho^2 \left(1 + d \frac{\Gamma_\rho}{m_\rho} \right), \quad (84a)$$

$$d = \frac{3m_\pi^2}{\pi k_\rho^2} \ln \left(\frac{m_\rho + 2k_\rho}{2m_\pi} \right) + \frac{m_\rho}{2\pi k_\rho} - \frac{m_\pi^2 m_\rho}{\pi k_\rho^3} \approx 0.48, \quad (84b)$$

$$D_1 = m_\rho^2 - s, \quad (84c)$$

$$D_2 = \Gamma_\rho \frac{m_\rho^2}{k_\rho^3} \left[k(s)^2 (h(s) - h_\rho) + k_\rho^2 h'(m_\rho^2) (m_\rho^2 - s) \right], \quad (84d)$$

$$D_3 = m_\rho \Gamma_\rho \left(\frac{k(s)}{k_\rho} \right)^3 \frac{m_\rho}{\sqrt{s}}, \quad (84e)$$

where h' denotes the derivative of h , and the functions k and h are defined as

$$k(s) = \frac{1}{2} \sqrt{s - 4m_\pi^2}, \quad h(s) = \frac{2}{\pi} \frac{k(s)}{\sqrt{s}} \ln \left(\frac{\sqrt{s} + 2k(s)}{2m_\pi} \right). \quad (85)$$

Furthermore, we use the short-hand notations $k_\rho = k(m_\rho^2)$ and $h_\rho = h(m_\rho^2)$. The interpretation is as follows: N is a normalization factor. D_1 is the dominant term in the denominator (in fact, for $D_2 = 0$, and constant D_3 , one would obtain a Lorentzian resonance profile for the π resonance). The term D_2 corrects the Lorentzian profile, while D_3 parameterizes the width of the π resonance. We use the following values from the latest data compilation of the Particle Data Group (see Ref. [53]),

$$\Gamma_\rho = 147.4(8) \text{ MeV}, \quad m_\rho = 775.26(23) \text{ MeV}, \quad (86)$$

and the charged pion mass $m_\pi = 139.57039(18) \text{ MeV}$.

Numerically, the contribution of the D_2 is smaller than that of D_1 . Hence, we can use the following approximation,

$$|F_\pi(s)|^2 = \frac{N^2}{(D_1 + D_2)^2 + (D_3)^2} \approx \frac{N^2}{(D_1)^2 + (D_3)^2}. \quad (87)$$

The difference of the results obtained with the approximation $D_2 = 0$, and without, is taken as the basis for an estimate of the theoretical uncertainty of the pionic contribution to hadronic vacuum polarization. The same approach was applied in Ref. [52]. However, one should note the following necessary corrections to Eq. (2.12) of Ref. [52],

$$\left(1 + \frac{\Gamma_\rho^d}{m_\rho} \right)^2 \rightarrow \left(1 + d \frac{\Gamma_\rho}{m_\rho} \right)^2, \quad (88a)$$

$$\left(\frac{s - 4m_\pi^2}{m_\rho^2 - 4m_\pi^2} \right)^{3/2} \rightarrow \left(\frac{s - 4m_\pi^2}{m_\rho^2 - 4m_\pi^2} \right)^3. \quad (88b)$$

The relative uncertainties based on this error estimate range from about 3% (for S states) to 11% (for the $4F$ state) for principal quantum numbers $n = 1, 2, 3, 4$.

We can now proceed to evaluate

$$E_\pi(nL) = \langle V_\pi(r) \rangle = \int dr r^2 [R_{nL}(r)]^2 V_\pi(r). \quad (89)$$

For example, for the $2P$ state of deuterium, one obtains the results

$$E_\pi(2P) = -4.1(2) \times 10^{-7} \text{ eV}, \quad (90)$$

which constitutes the dominant hadronic VP correction to the energy of this state.

For ω and ϕ mesons, it is adequate to use the pole approximation,

$$\rho_p(s) = \frac{4\pi^2}{f_p^2} \delta(s - m_p^2), \quad (91)$$

where the subscript p designates the particle being considered. After Fourier transformation, one can express the vacuum polarization potential due to the resonance with particle p as a Yukawa potential, with a specific coupling parameter,

$$V_p(r) = -\frac{\alpha}{\pi} \frac{4\pi^2}{f_p^2} \frac{\alpha}{r} e^{-m_p r}. \quad (92)$$

We can use the parameters

$$\frac{f_\omega^2}{4\pi} = 18(2), \quad \frac{f_\phi^2}{4\pi} = 11(2) \quad (93)$$

(see Refs. [52, 54]) and the mass values $m_\omega = 782.66(13) \text{ MeV}$, $m_\phi = 1019.461(16) \text{ MeV}$ of Refs. [26, 27]. The hadronic vacuum-polarization potential $V_p(r)$ due to one of the ω and ϕ mesons leads to the energy shift

$$E_p(nL) = \langle V_p(r) \rangle = \int dr r^2 [R_{nL}(r)]^2 V_p(r). \quad (94)$$

The contribution of the high-energy background above 1 GeV can be estimated, in the dispersive approach, on the basis of the spectral function

$$\rho(s) = \frac{R}{3s}, \quad m_1 < \sqrt{s} < m_2, \quad (95)$$

where R is the ratio of a virtual photon going into a hadronic pair, to a virtual photon going into a light fermion pair [40]. Assuming R to be piecewise constant is a permissible approximation, because, according to Ref. [40],

$$R \approx \begin{cases} R_2 = 2 & m_1 \equiv 1 \text{ GeV} < \sqrt{s} < m_2 \equiv 4 \text{ GeV} \\ R_4 = 4 & m_2 \equiv 4 \text{ GeV} < \sqrt{s} < \infty \end{cases}. \quad (96)$$

According to Fig. 18 of Ref. [55], the approximation (96) still represents a suitable approximation to the additional, recently available experimental data in the relevant energy domain. Hence, the vacuum polarization potential describing the high-energy background for $m_1 < \sqrt{s} < m_2$ is (in momentum space)

$$V_{m_1, m_2}(\vec{k}) = -\frac{\alpha}{\pi} \int_{(m_1)^2}^{(m_2)^2} ds \frac{R}{3s} \frac{4\pi\alpha}{\vec{k}^2 + s}. \quad (97)$$

After Fourier transformation, the potential becomes

$$V_{m_1, m_2}(r) = \frac{\alpha}{\pi} \left(-\frac{\alpha}{r}\right) \frac{2R}{3} \left[\text{Ei}(-m_2 r) - \text{Ei}(-m_1 r) \right]. \quad (98)$$

Here, the exponential integral $\text{Ei}(z)$ is given as follows,

$$\text{Ei}(z) \equiv - \int_{-z}^{\infty} \frac{dt}{t} e^{-t}. \quad (99)$$

The hadronic vacuum polarization potential due to the high-energy background can thus be approximated as

$$V_b(r) = \frac{\alpha}{\pi} \left(-\frac{2\alpha}{3r}\right) \left[R_2 \left\{ \text{Ei}(-m_2 r) - \text{Ei}(-m_1 r) \right\} + R_4 \left\{ 0 - \text{Ei}(-m_2 r) \right\} \right], \quad (100)$$

leading to the energy shift

$$E_b(nL) = \langle V_b(r) \rangle = \int dr r^2 [R_{nL}(r)]^2 V_b(r), \quad (101)$$

which can easily be evaluated numerically.

According to Eqs. (89), (94), and (101), the result for the hadronic vacuum polarization energy shift $E_{\text{had}}(r)$ is

$$E_{\text{had}}(nL) = E_{\pi}(nL) + E_{\omega}(nL) + E_{\phi}(nL) + E_b(nL). \quad (102)$$

For the states of interest for the current investigation, one obtains

$$E_{\text{had}}(2P) = -4.8(5) \times 10^{-4} \text{ meV}, \quad (103a)$$

$$E_{\text{had}}(3P) = -1.7(2) \times 10^{-4} \text{ meV}, \quad (103b)$$

$$E_{\text{had}}(3D) = -2.9(3) \times 10^{-9} \text{ meV}, \quad (103c)$$

$$E_{\text{had}}(4P) = -7.5(8) \times 10^{-5} \text{ meV}, \quad (103d)$$

$$E_{\text{had}}(4D) = -1.8(2) \times 10^{-9} \text{ meV}, \quad (103e)$$

$$E_{\text{had}}(4F) = -1.8(2) \times 10^{-14} \text{ meV}. \quad (103f)$$

We have included an uncertainty of about 10%, as suggested by the effect of the approximation (87) in the pion contribution, the simplicity of our approximations, and the size of the error in the estimate of the hadronic VP contribution to the muon anomalous moment, as described below. These energy corrections are small compared to other contributions of order α^3 or α^4 .

B. Hadronic VP: Verification

In order to verify our approximate approach for the treatment of hadronic vacuum-polarization, we have carried out a calculation of the corresponding contribution to the muon anomalous magnetic moment a_{μ} . The leading two-loop hadronic contribution to the muon anomalous magnetic moment is [46, 56, 57]

$$\delta a_{\mu, \text{had}} = \left(\frac{\alpha}{\pi}\right)^2 \int_{s_0}^{\infty} ds K_{\mu}(s) \rho_{\text{had}}(s), \quad (104)$$

where the kernel function is

$$K_{\mu}(s) = \int_0^1 dx \frac{x^2(1-x)}{x^2 + (1-x)s/m_{\mu}^2}. \quad (105)$$

As a check of the formulas, we consider the replacements $m_{\mu} \rightarrow m_e$ and

$$\rho_{\text{had}}(s) \rightarrow \rho_e(s) = \frac{1}{\alpha s} \text{Im} \left[\Pi_R^{(1)}(s) \right] = \frac{v(1-v^2/3)}{2s} \quad (106)$$

in Eqs. (104) and (105). With those replacements, one obtains the known contribution to the electron anomalous moment due to one-loop electron vacuum polarization (see p. 852 of Ref. [58]),

$$\delta a_{e, \text{eVP}} = \left(\frac{\alpha}{\pi}\right)^2 \left(\frac{119}{36} - \frac{\pi^2}{3} \right). \quad (107)$$

We use the formula $\rho_{\text{had}}(r) = \rho_{\pi}(r) + \rho_{\omega}(r) + \rho_{\phi}(r) + \rho_b(r)$ for the spectral density of hadronic vacuum polarization and Eq. (104) to obtain the hadronic VP contribution to the muon anomalous moment. We find

$$\begin{aligned} a_{\mu, \text{had}} &= \underbrace{4.39 \times 10^{-8}}_{\pi^+ \pi^-} + \underbrace{0.50 \times 10^{-8}}_{\omega \text{ meson}} \\ &\quad + \underbrace{0.51 \times 10^{-8}}_{\phi \text{ meson}} + \underbrace{1.35 \times 10^{-8}}_{\text{background}} \\ &= 6.75 \times 10^{-8}. \end{aligned} \quad (108)$$

The difference between this value and the value of $a_{\mu, \text{had}} = 6.93 \times 10^{-8}$ given in Ref. [55] is roughly 3%. The high degree of agreement between our result and the result of more careful evaluations supports the assumption of the general validity of our simplified approach (and the smallness of the corresponding energy correction).

C. Finite-Size Effect

The deuteron has a finite size; its root-mean-square (RMS) charge radius is $r_d = 2.12778(27) \text{ fm}$. So, the interaction between deuteron and antideuteron is not really that between two point-like particles. The fact that the charge is spread out means that the average potential will not be quite as negative as it would be were the

TABLE V. Finite-size and strong-interaction energy shifts for deuteronium states. Shown are the exact energy shifts [see Eq. (117)] between a pointlike Coulomb system and a system with one particle being a uniformly charged sphere (doubled because both particles have finite size), the same energy shifts calculated perturbatively [see Eq. (118)], the Breit energy shifts E_D proportional to r_d^2 [see Eq. (119)], and the strong interaction energy shifts E_S [see Eq. (132)]. The uncertainties in the strong interaction shifts are estimated to be 100% of their value. All energies are given in meV.

Level nL	$E_{\text{FS}}^{\text{exact}}$ (meV)	$E_{\text{FS}}^{\text{pert}}$ (meV)	E_D (meV)	E_S (meV)
1S	3.19×10^5	3.37×10^5	3.63×10^5	3.46×10^6
2S	4.00×10^4	4.21×10^4	4.53×10^4	4.33×10^5
2P	5.83	5.87	0	130
3S	1.19×10^4	1.25×10^4	1.34×10^4	1.28×10^5
3P	2.05	2.06	0	45.7
3D	3.00×10^{-5}	3.01×10^{-5}	0	5.09×10^{-4}
4S	5.00×10^3	5.26×10^3	5.67×10^3	5.41×10^4
4P	0.911	0.918	0	20.3
4D	1.80×10^{-5}	1.81×10^{-5}	0	3.06×10^{-4}
4F	5.73×10^{-11}	5.74×10^{-11}	0	5.11×10^{-10}

particles pointlike, so the binding energy will be less in magnitude that it would be for pointlike particles. That is, the energy correction due to the finite size of the particles will be positive. We can make an estimate of the size of this correction by calculating the interaction energy for two uniformly charged spheres of radius r_d . This estimate is fully sufficient for our purposes, because the nuclear-structure effects are numerically dominated by the strong-interaction correction discussed in Sec. V E.

Consider first the case of a pointlike particle of mass m_1 and charge $q_1 = -e$ in the field of a uniformly charged spherical shell of radius r_d , mass m_2 , and charge $q_2 = e$. The Schrödinger equation describing this situation is

$$-\frac{1}{2m_r}\nabla^2\psi(\vec{r}) + V(r)\psi(\vec{r}) = E\psi(\vec{r}), \quad (109)$$

where

$$V(r) = \begin{cases} -\frac{\alpha}{r_d} & \text{if } r < r_d \\ -\frac{\alpha}{r} & \text{if } r > r_d \end{cases}. \quad (110)$$

We write $\psi(\vec{r}) = R_{\nu L}(r) Y_{Lm}(\theta, \varphi)$ and $R_{\nu L}(r) = \frac{u_{\nu L}(r)}{r}$. In terms of $u_{\nu L}(r)$, the radial equation is

$$-\frac{1}{2m_r}\frac{d^2}{dr^2}u_{\nu L}(r) + \left(V(r) + \frac{L(L+1)}{2m_r r^2}\right)u_{\nu L}(r) = E_{\nu} u_{\nu L}(r). \quad (111)$$

We define ν so that the energy eigenvalue is $E_{\nu} = -\frac{m_r\alpha^2}{2\nu^2}$, and define a scaled radial variable ρ with

$$\rho = \sqrt{-8m_r E_{\nu}} r = \frac{2m_r\alpha}{\nu} r. \quad (112)$$

In terms of ρ , the sphere boundary is at $\rho_d = \frac{\kappa}{\nu}$, with $\kappa = \frac{2r_d}{a_0}$ where $a_0 = \frac{1}{m_r\alpha}$ is the Bohr radius. Numerically, one has $a_0 = 28.834\,200\,570(10)$ (see Table I) and $\kappa = 0.147587$. For $\rho < \rho_d$, the radial equation becomes

$$\left(\frac{d^2}{d\rho^2} - \frac{L(L+1)}{\rho^2} + \frac{\nu^2}{\kappa} - \frac{1}{4}\right)u_{\nu L}(\rho) = 0, \quad (113)$$

and for $\rho > \rho_d$ it is

$$\left(\frac{d^2}{d\rho^2} - \frac{L(L+1)}{\rho^2} + \frac{\nu}{\rho} - \frac{1}{4}\right)u_{\nu L}(\rho) = 0. \quad (114)$$

The solution for Eq. (113) that is finite as $\rho \rightarrow 0$ is

$$u_{\nu L}(\rho) = \sqrt{\rho} J_{L+1/2}\left(\rho\sqrt{\frac{\nu^2}{\kappa} - \frac{1}{4}}\right), \quad (115)$$

where $J_{\ell}(r)$ is a Bessel function of the first kind, and the solution for Eq. (114) that is finite as $\rho \rightarrow \infty$ is

$$u_{\nu L}(\rho) = W_{\nu, L+1/2}(\rho), \quad (116)$$

where $W_{\nu, \ell}(r)$ is a Whittaker W function. Continuity of the wave function and its first derivative at $\rho = \rho_d$ requires the continuity of the derivative of the logarithm $\ln[u_{\nu L}(\rho)]$. Upon solving this continuity equation for a given L and for $\nu \approx n$, one finds the appropriate value of ν to use in the energy $E_{\nu} = -\frac{m_r\alpha^2}{2\nu^2}$. The finite-size energy correction is thus

$$E_{\text{FS}}^{\text{exact}} = E_{\nu} - E_n = -\frac{m_r\alpha^2}{2}\left(\frac{1}{\nu^2} - \frac{1}{n^2}\right). \quad (117)$$

For deuterium, this expression must be doubled since both deuteron and antideuteron have extension.

One could also approach the finite size correction perturbatively, with a perturbing potential

$$\delta V(r) = \left(-\frac{\alpha}{r_d} + \frac{\alpha}{r} \right) \Theta(r < r_d), \quad (118)$$

where Θ is the Heaviside step function. Results for the perturbative shifts $E_{\text{FS}}^{\text{pert}}$ are given in Table V.

We have already obtained a “finite-size” effect in our calculation of the Breit correction, namely the r_d term in E_{BR} . This term is

$$E_{\text{D}} = \frac{\alpha^4 m_d \tilde{r}_d^2}{6n^3} \delta_{L,0} \quad (119)$$

where $\tilde{r}_d = m_d r_d / (\hbar c) \approx 20.2248(26)$ [see Eq. (12)]. The Breit finite-size correction E_{D} vanishes for $L > 0$. The calculation above shows how the extended deuteron charge distribution affects states with $L > 0$. Due to the small size of r_d/a_0 , which equals 0.0738, the finite size correction decreases rapidly as L increases.

Numerical results for deuterium states with $n = 1, 2, 3, 4$ are shown in Table V. The numerical values obtained from the perturbative calculation ($E_{\text{FS}}^{\text{pert}}$) are consistent with the exact results from actually solving the differential equation and finding the energy eigenvalue ($E_{\text{FS}}^{\text{exact}}$) for all states. The Breit contribution E_{D} is roughly consistent with those two for S states, but misses the small corrections for non- S states.

D. Deuteron Polarizability

The deuteron can be deformed by an external electric field. The extent of this deformation is described by polarizability constants. For the (static) scalar and tensor polarizabilities of the deuteron, we use the calculated results of Friar and Payne [59],

$$\alpha_E = 0.6330(13) \text{ fm}^3, \quad (120a)$$

$$\tau_d = 0.0317(3) \text{ fm}^3. \quad (120b)$$

These constants enter the polarizability tensor $(\alpha_P)^{ij}$ of the deuteron, which is expressed as

$$(\alpha_P)^{ij} = \alpha_E \frac{\delta^{ij}}{3} + i \sigma_d \epsilon^{ijk} \frac{S^k}{2} + \tau_d (S^i S^j)^{(2)}. \quad (121)$$

Here, the constants α_E , σ_d and τ_d parameterize the electric scalar ($\ell = 0$), vector ($\ell = 1$) and tensor ($\ell = 2$) components of the deuteron’s polarizability, respectively. These results are expressed in terms of a polarization volume, *i.e.*, in units of fermi cubed. Temporarily restoring SI units according to standard procedures [60], we indicate the conversion of the polarization volume to the (static) SI polarizability, which, for the scalar polarizability, reads as follows,

$$\alpha_{E,\text{SI}} = 4\pi\epsilon_0 \alpha_{E,\text{vol}}, \quad (122)$$

where ϵ_0 is the vacuum permittivity. For a recent overview of the use of the SI polarizability (units are those of a dipole moment squared divided by an energy) in a related context, see Ref. [61]. The numerical values in Eq. (120) thus have to be interpreted in terms of volume polarizabilities.

Measurements of the deuteron scalar polarizability were made by two groups and date a few decades back. The first is by Rodning *et al.* in 1982 (see Ref. [62]). They give references to six prior theoretical calculations of the deuteron polarizability with values ranging from 0.21 fm^3 to 0.64 fm^3 , with a best estimate close to 0.60 fm^3 . They measured a value (from now on, we assume that all polarizabilities are indicated in the “volume” conventions)

$$\alpha_E = 0.70(5) \text{ fm}^3, \quad (123)$$

based on elastic scattering of deuterons on lead. A second experimental value was reported by Friar *et al.* in 1983 (see Ref. [63]), based on deuteron photoabsorption data, a dispersion relation and other theoretical input, and a number of corrections. Their result was

$$\alpha_E = 0.64(5) \text{ fm}^3. \quad (124)$$

A weighted average of these two values is

$$\alpha_E = 0.645(32) \text{ fm}^3, \quad (125)$$

which is consistent with the calculated value of Eq. (120a). To the best of our knowledge, there are currently no experimental values available for the deuteron’s tensor polarizability.

A comprehensive derivation of the polarizability correction of an atomic core for non- S states of a bound system is presented in Sec. 6.6 of Ref. [6]. Because the focus in the current work is on S states, we adopt this treatment here. A generalization of Eq. (6.177) of Ref. [6] to account for the tensor structure of the polarizability, and also accounting for the two polarizable constituent particles, allows us to find the polarizability contribution to the interaction Hamiltonian

$$\begin{aligned} H_P &= -\frac{\alpha}{2} \frac{\hat{x}^i}{r^2} \left[3\alpha_P^{ij}(d) + 3\alpha_P^{ij}(\bar{d}) \right] \frac{\hat{x}^j}{r^2} \\ &= -\frac{\alpha}{2} \left\{ 2\alpha_E \delta^{ij} + 3\tau_P [(S_+^i S_+^j)^{(2)} + (S_-^i S_-^j)^{(2)}] \right\} \frac{\hat{x}^i \hat{x}^j}{r^4} \\ &= -\alpha_E \frac{\alpha}{r^4} - \frac{3}{2} \tau_P [(S_+^i S_+^j)^{(2)} + (S_-^i S_-^j)^{(2)}] (\hat{x}^i \hat{x}^j)^{(2)} \frac{\alpha}{r^4} \\ &\equiv H_{\text{PS}} + H_{\text{PT}}. \end{aligned} \quad (126)$$

Here, H_P is the sum of scalar (H_{PS}) and tensor (H_{PT}) components. Throughout the above derivation, we have converted the static polarizability $\alpha(\omega = 0)$ used in Eq. (6.177) of Ref. [6] to a volume polarizability by dividing by 4π .

The energy correction due to the scalar polarizability factor is

$$\begin{aligned} E_{\text{PS}} &= -\alpha_E \left\langle \frac{\alpha}{r^4} \right\rangle \\ &= -\frac{\tilde{\alpha}_E E_0 \alpha^3 [3n^2 - L(L+1)]}{L(L+1)(2L-1)(2L+1)(2L+3)n^5}, \end{aligned} \quad (127)$$

where E_0 is given in Table I, and $\tilde{\alpha}_E$ is the dimensionless scalar polarizability factor,

$$\tilde{\alpha}_E = m_d^3 \alpha_E = \frac{(m_d c^2)^3 \alpha_E}{(\hbar c)^3} = 543.6(1.1). \quad (128)$$

We used Eq. (4.346d) of Ref. [6] for the expectation value of $1/r^4$. Results for the scalar polarizability energy corrections are tabulated in Table IV. Due to the large size of $\tilde{\alpha}_E$, the order- α^5 scalar polarizability contributions are comparable in size to the α^4 contributions listed in Table IV for the states considered.

The matrix elements of the tensor polarizability Hamiltonian involve the $D_{LS'SJ}$ angular factor found in (32). One has

$$(H_{PT})_{nLS'SJ} = -\frac{3\tilde{\tau}_P E_0 \alpha^3 D_{LS'SJ} [3n^2 - L(L+1)]}{2L(L+1)(2L-1)(2L+1)(2L+3)n^5}, \quad (129)$$

where the dimensionless tensor polarizability factor is

$$\tilde{\tau}_P = m_d^3 \tau_P = \frac{(m_d c^2)^3 \tau_P}{(\hbar c)^3} = 27.2(0.3). \quad (130)$$

The tensor polarizability shifts (using the calculated value of τ_P) are relatively small compared to the Breit energy corrections due to the extra factor of α . For example, the shifts for the 4^3D_J levels are

$$E_{PT}(4^3D_1) = -0.00860(8), \quad (131a)$$

$$E_{PT}(4^3D_2) = 0.00860(8), \quad (131b)$$

$$E_{PT}(4^3D_3) = -0.00246(3), \quad (131c)$$

which are small compared to the corresponding Breit shifts from Table III. Contributions of this size should be noticeable in the data given precise enough measurements of the $4F \rightarrow 4D$ transition energies.

E. Strong Interaction Correction

Just as in protonium [2], the strong interaction modifies the deuteron-antideuteron interaction at short distances of about 1 fm (the effective range of the strong interaction) in a way that is easily estimated. One can assume that the probability density vanishes for distances $r \lesssim 1$ fm due to strong interaction mediated annihilation (see the comprehensive discussion in Sec. 3.12 of Ref. [2] for protonium). Hence, we treat the problem as if there was a hard cutoff at $a = a_{\text{had}} = 1$ fm. We estimate the effect based on the Deser–Trueman formula [2, 21–25], for which a suitable generalization to excited states has recently been found in Ref. [25]. We find [25] that the non-relativistic energy levels in the cut-off potential are shifted from their pure Coulomb values by the positive amount

$$E_S = \frac{2\alpha_{nL}\beta_L}{n^3} \left(\frac{a}{a_0}\right)^{2L+1} \alpha^2 m_r, \quad (132)$$

where a_0 is the deuteronium Bohr radius given in Table I, and

$$\alpha_{nL} = \prod_{s=1}^L \left(\frac{1}{s^2} - \frac{1}{n^2} \right), \quad \beta_L = \frac{2L+1}{[(2L+1)!!]^2} \quad (133)$$

with $\alpha_{n0} \equiv 1$. Corresponding results are entered in Tables IV and V. We conservatively estimate their uncertainty as 100% of the obtained results. The S -wave scattering length generalizes the concept of the hard-sphere radius a_h for general electromagnetically bound systems with orbiting hadrons [2, 21–25]. Our estimate, given in Eq. (132), is supported by relatively recent investigations which indicate that the scattering length, as compared to protonium, is a decreasing function of the atomic weight (see the conclusions of Ref. [64]). The strong-interaction shifts follow the same general pattern as a function of L as the finite-size corrections of the previous section, and are even more drastically suppressed for higher angular momenta in view of the squared double factorial $[(2L+1)!!]^2$ in the denominator of Eq. (132). Still, for typical states under investigation here, they are larger than the finite-size corrections by an order of magnitude.

VI. DIPOLE TRANSITIONS

A. General Properties of the Spectrum

Our investigations have revealed that in deuteronium, a bound system with two spin-1 particles, the spin-dependent (hyper)fine structures are composed very differently in comparison to bound systems where the orbiting particles have half-integer spin (*e.g.*, positronium). However, there are also similarities: Namely, just as in positronium, the spin-dependent corrections in deuteronium all have the same order-of-magnitude ($\alpha^4 m_d$). We have studied, in Sec. IV, the leading radiative corrections (one-loop and two-loop eVP) for the lowest non- S levels in the bound system. For states with the same principal quantum number n , the dominant radiative correction (one-loop eVP) to the energy is more strongly negative (hence, more attractive) for states low orbital angular momenta, leading to the dominant contribution to the Lamb shift in the bound system.

B. Selection Rules

One aspect we have not treated so far in this work concerns selection rules for dipole transitions. Here we work out the selection rules for electric dipole transitions. The interaction operator is proportional to $\vec{r} \cdot \vec{E}$. The electric field acts to create a photon—our concern is with the position operator \vec{r} , which involves the variables of the deuteronium state. Specifically, we find that single-photon electric dipole transitions are allowed between states with quantum numbers $n_1, L_1, S_1, J_1, J_{z1}$

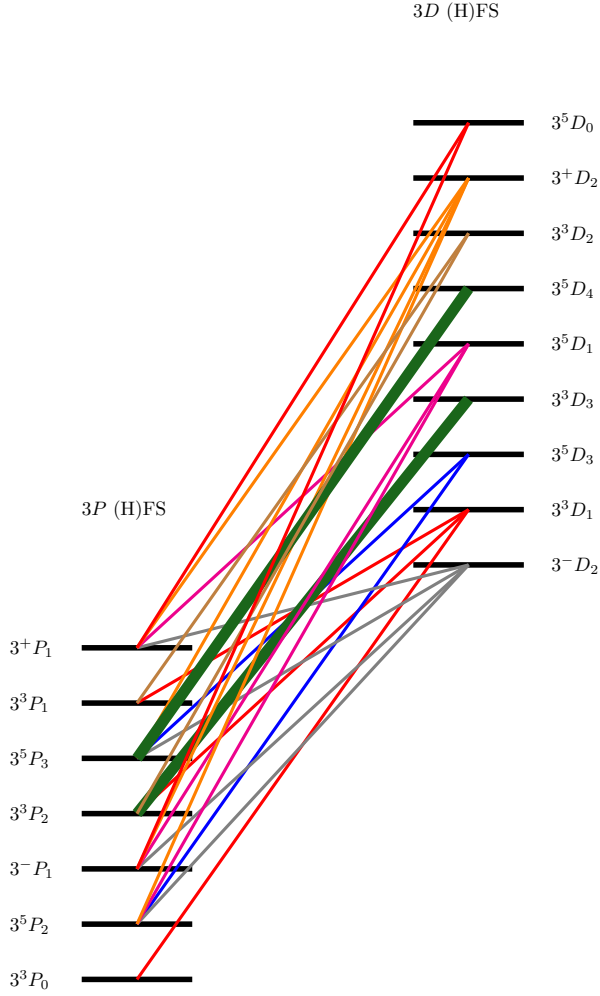


FIG. 2. The dipole-allowed $3D$ - $3P$ transitions are displayed graphically. The transitions are resolved with respect to the (hyper)fine-structure of the levels [denoted as (H)FS]. When the upper sublevel undergoes only one dipole-permitted transition, we use thick lines. Others transitions are denoted by ordinary solid lines. The viewgraph illustrates the much more complex (hyper)fine-structure that is encountered in the bound system of two spin-1 particles, as compared to bound systems involving a light spin-1/2 particle orbiting a heavy nucleus.

and $n_2, L_2, S_2, J_2, J_{z2}$ (where J_z represents the magnetic quantum number of the total angular momentum) when

$$\langle n_2, L_2, S_2, J_2, J_{z2} | (\vec{r})_{1,m} | n_1, L_1, S_1, J_1, J_{z1} \rangle \neq 0. \quad (134)$$

Here, $(\vec{r})_{1,m}$ is the spherical tensor of rank one (and spherical component $m = -1, 0, 1$) corresponding to the position vector \vec{r} . It is immediately clear from the general rules of addition of angular momentum that a state with total angular momentum J_1 and z component J_{z1} , acted on by an operator with angular momentum one and z component m , only has overlap with a state of total angular momentum $J_2 = J_1 \pm 1$ or $J_2 = J_1$, and

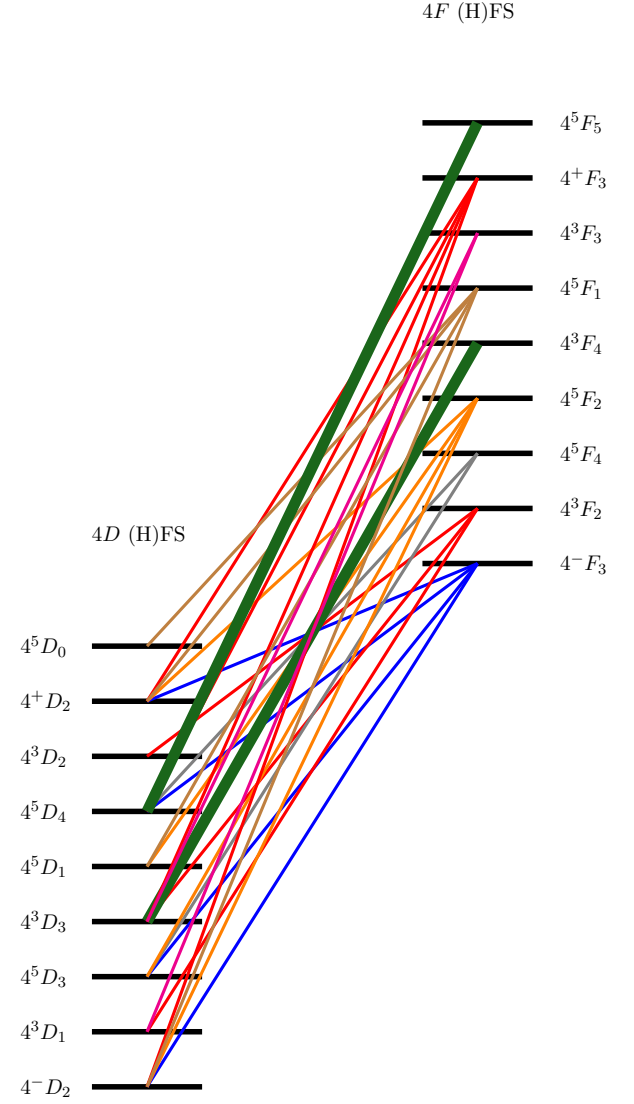


FIG. 3. Same as the viewgraph Fig. 2, but for the dipole-allowed $4F$ - $4D$ transitions.

$J_{z2} = J_{z1} + m$. In addition, parity conservation implies that $(-1)^{L_2} = (-1)^{L_1+1}$. Additional conditions can be found by looking more deeply into the condition (134). The states, as given in (3), have the form

$$\psi_{nLSJM}(\vec{r}) = R_{nL}(r) \Xi_{JM}^{LS}(\theta, \varphi) \quad (135)$$

where

$$\Xi_{JM}^{LS}(\theta, \varphi) = \sum_{M_L, M_S} C_{LM_L; SM_S}^{JM} Y_{LM_L}(\theta, \varphi) \chi_{SM_S}, \quad (136)$$

where χ_{SM_S} is the spin-state of deuteronium, built from two spin-one constituents. Also, one has $(\hat{r})_{1m} = \sqrt{\frac{3}{4\pi}} Y_{1m}(\theta, \varphi)$. Hence, the angular part of Eq. (134) is

TABLE VI. Energies and wavelengths for $3D \rightarrow 3P$ transitions in deuterium. The uncertainties for all of these transitions are dominated by the strong interaction $3P$ state uncertainty of 0.046 eV.

transition	energy ΔE (eV)	wavelength λ (nm)
$3^-D_2 \rightarrow 3^-P_1$	1.342(46)	924(32)
$3^-D_2 \rightarrow 3^+P_1$	0.936(46)	1325(65)
$3^-D_2 \rightarrow 3^5P_2$	1.345(46)	922(32)
$3^-D_2 \rightarrow 3^5P_3$	1.134(46)	1093(45)
$3^+D_2 \rightarrow 3^-P_1$	1.410(46)	879(29)
$3^+D_2 \rightarrow 3^+P_1$	1.003(46)	1236(57)
$3^+D_2 \rightarrow 3^5P_2$	1.412(46)	878(29)
$3^+D_2 \rightarrow 3^5P_3$	1.202(46)	1032(40)
$3^3D_1 \rightarrow 3^3P_0$	1.452(46)	854(27)
$3^3D_1 \rightarrow 3^3P_1$	1.105(46)	1123(47)
$3^3D_1 \rightarrow 3^3P_2$	1.219(46)	1017(39)
$3^3D_2 \rightarrow 3^3P_1$	1.153(46)	1075(43)
$3^3D_2 \rightarrow 3^3P_2$	1.268(46)	978(36)
$3^3D_3 \rightarrow 3^3P_2$	1.245(46)	996(37)
$3^5D_0 \rightarrow 3^-P_1$	1.411(46)	878(29)
$3^5D_0 \rightarrow 3^+P_1$	1.005(46)	1234(57)
$3^5D_1 \rightarrow 3^-P_1$	1.410(46)	879(29)
$3^5D_1 \rightarrow 3^+P_1$	1.003(46)	1236(57)
$3^5D_1 \rightarrow 3^5P_2$	1.412(46)	878(29)
$3^5D_3 \rightarrow 3^5P_2$	1.363(46)	910(31)
$3^5D_3 \rightarrow 3^5P_3$	1.152(46)	1076(43)
$3^5D_4 \rightarrow 3^5P_3$	1.195(46)	1038(40)

proportional to

$$\sum_{M_{L_1}, M_{L_2}, M_{S_1}, M_{S_2}} C_{L_2 M_{L_2}; S_2 M_{S_2}}^{J_2 J_{z2}} C_{L_1 M_{L_1}; S_1 M_{S_1}}^{J_1 J_{z1}} \times \int d\Omega Y_{L_2 M_{L_2}}^*(\theta, \varphi) Y_{1m}(\theta, \varphi) Y_{L_1 M_{L_1}}(\theta, \varphi) \times \langle \chi_{S_2 M_{S_2}}^\dagger \cdot \chi_{S_1 M_{S_1}} \rangle. \quad (137)$$

Here, we denote the scalar product of the spin states by a central dot (\cdot) , for absolute clarity. The spin inner product enforces the selection rule $S_2 = S_1$. The integral over the solid angle can be done for general quantum numbers [see Eq. (6.64) of [6]] and contains the $3J$ symbol

$$\begin{pmatrix} L_2 & 1 & L_1 \\ 0 & 0 & 0 \end{pmatrix} \quad (138)$$

as a factor, which vanishes unless $L_2 = L_1 \pm 1$. As a result, the selection rules for single-photon electric dipole

TABLE VII. Energies and wavelengths for $4F \rightarrow 4D$ transitions in deuterium. The uncertainties for these transitions arise from the uncertainty in the quadrupole moment Q_d and the strong interaction uncertainty for $4D$ states (see Tables III and V).

transition	energy ΔE (meV)	wavelength λ (nm)
$4^-F_3 \rightarrow 4^-D_2$	314.9049(15)	3937.19(2)
$4^-F_3 \rightarrow 4^+D_2$	286.4151(14)	4328.83(2)
$4^-F_3 \rightarrow 4^5D_3$	307.2340(12)	4035.50(2)
$4^-F_3 \rightarrow 4^5D_4$	289.4061(10)	4284.091(15)
$4^+F_3 \rightarrow 4^-D_2$	324.9899(14)	3815.02(2)
$4^+F_3 \rightarrow 4^+D_2$	296.5000(14)	4181.59(2)
$4^+F_3 \rightarrow 4^5D_3$	317.3190(12)	3907.242(15)
$4^+F_3 \rightarrow 4^5D_4$	299.4910(10)	4139.830(14)
$4^3F_2 \rightarrow 4^3D_1$	312.2642(11)	3970.490(14)
$4^3F_2 \rightarrow 4^3D_2$	291.6724(11)	4250.80(2)
$4^3F_2 \rightarrow 4^3D_3$	301.3068(9)	4114.882(12)
$4^3F_3 \rightarrow 4^3D_2$	298.6482(11)	4151.51(2)
$4^3F_3 \rightarrow 4^3D_3$	308.2826(9)	4021.771(11)
$4^3F_4 \rightarrow 4^3D_3$	304.9837(8)	4065.273(11)
$4^5F_1 \rightarrow 4^5D_0$	295.845(2)	4190.86(3)
$4^5F_1 \rightarrow 4^5D_1$	296.5000(12)	4181.59(2)
$4^5F_1 \rightarrow 4^-D_2$	324.9899(15)	3815.02(2)
$4^5F_1 \rightarrow 4^+D_2$	296.5000(15)	4181.59(2)
$4^5F_2 \rightarrow 4^5D_1$	292.4153(11)	4240.00(2)
$4^5F_2 \rightarrow 4^-D_2$	320.9051(14)	3863.58(2)
$4^5F_2 \rightarrow 4^+D_2$	292.4153(14)	4240.00(2)
$4^5F_2 \rightarrow 4^5D_3$	313.2342(12)	3958.195(15)
$4^5F_4 \rightarrow 4^5D_3$	311.1198(12)	3985.096(15)
$4^5F_4 \rightarrow 4^5D_4$	293.2918(9)	4227.332(14)
$4^5F_5 \rightarrow 4^5D_4$	299.8126(9)	4135.389(13)

transitions are

$$J_2 = J_1 \pm 1 \text{ or } J_2 = J_1, \quad L_2 = L_1 \pm 1, \quad S_2 = S_1. \quad (139)$$

The dipole allowed $3D-3P$ and $4F-4D$ transitions are displayed graphically in Figs. 2 and 3. Transition energies and wavelengths are shown in Tables VI and VII.

VII. CONCLUSIONS

The bound system of a deuteron and its antiparticle offers some unique elements in comparison with other two-body bound states where the partners have equal mass. In comparison to positronium [65–67], deuterium of-

fers drastically enhanced characteristic field strengths, which allow the study of QED effects under extreme conditions. In comparison to protonium [1, 2], deuterium offers the added complexity of the spin-1 character of the bound particles, which opens the door for an investigation of the much more complex QED of spin-1 particles as compared to the well-understood spin-1/2 case. In comparison to dimuonium (or, true muonium, see Refs. [40, 41, 68, 69]), deuterium offers the enhanced stability of the deuteron, which does not decay on a scale of microseconds (like the muon and antimuon). Hence, the deuterium bound system offers unique characteristics for a detailed study of QED effects of spin-1 particles in combination with highly nontrivial spin-induced relativistic effects and radiative (vacuum polarization) corrections.

Here, we have evaluated the dominant features of the spectrum of deuterium. The main terms are the non-relativistic Schrödinger–Coulomb energy (order $\alpha^2 m_d$) and the one-loop eVP correction (order $\alpha^3 m_d$). The dominant spin dependence is contained in the Breit corrections (order $\alpha^4 m_d$, see Sec. III). The muonic VP is enhanced in deuterium (see Sec. IV B), and reducible as well as irreducible eVP corrections are well under control (see Secs. IV C–IV E). In Sec. V, we have demonstrated that strong-interaction and internal-structure effects do not represent obstacles to a detailed study of the very interesting spin-induced relativistic and radiative ef-

fects. Namely, for non- S states, the hadronic VP effect are numerically small (see Secs. V A and V B). Finite-size effects can be treated perturbatively and are likewise numerically small for states with $L \geq 2$ (see Sec. V C). Strong-interaction corrections can be obtained on the basis of the generalized Deser-Trueman formula [2, 21–25].

Certain Lamb shift transitions in deuterium are in the optical or infrared range and are easily accessible by laser spectroscopy. Two very attractive transitions appears to be the $3D-3P$ and $4F-4D$ Lamb shift transitions, which are analyzed (with their dipole-allowed (hyper)fine-structure components in Figs. 2 and 3. (See also Tables VI and VII.) An additional important conclusion of our investigations is that internal-structure corrections, for the mentioned transitions, are numerically suppressed and do not preclude precision experiments on the bound system of a deuteron and its antiparticle.

ACKNOWLEDGMENTS

The authors acknowledge insightful discussions with Daniel Murtagh and Professor Jean-Marc Richard. This work was supported by the National Science Foundation through Grants PHY-2308792 (G.S.A.) and PHY-2110294 (U.D.J.), and by the National Institute of Standards and Technology Grant 60NANB23D230 (G.S.A.).

Appendix A: Tensor Structures

We investigate some angular structures relevant to the discussion. Let $X^{(2)ij}$ and $S^{(2)ij}$ be two symmetric traceless second-rank Cartesian tensors, with $i, j = x, y, z$,

$$X^{(2)ij} = X^{(2)ji}, \quad X^{(2)ii} = 0, \quad S^{(2)ij} = S^{(2)ji}, \quad S^{(2)ii} = 0. \quad (\text{A1})$$

The Einstein summation convention has been used. The corresponding spherical tensors are denoted as X_{Lm} and S_{Lm} with $L = 2$. We match the Cartesian against the spherical forms by considering Eq. (6.28c) of Ref. [6],

$$X_{20} = \sqrt{\frac{3}{2}} X^{(2)33}, \quad S_{20} = \sqrt{\frac{3}{2}} S^{(2)33}. \quad (\text{A2})$$

We denote Cartesian indices as superscripts, while spherical tensor indices are denoted by subscripts. The prefactor $\sqrt{3/2}$ follows from the use of the Clebsch–Gordan coefficients, as explained in Chap. 6 of Ref. [6]. Of particular interest for us are the second-rank tensors defined in terms of Cartesian vector components of the underlying vectors:

$$X^{(2)ij} = (\hat{x}^i \hat{x}^j)^{(2)} = \hat{x}^i \hat{x}^j - \frac{1}{3} \delta^{ij}, \quad S_{ab}^{(2)ij} = (S_a^i S_b^j)^{(2)} = \frac{1}{2} (S_a^i S_b^j + S_a^j S_b^i) - \frac{1}{3} \delta^{ij} \vec{S}_a \cdot \vec{S}_b. \quad (\text{A3})$$

The latter is assumed to be the rank-two tensor constructed from \vec{S}_a and \vec{S}_b . The corresponding spherical tensors are normalized according to Eq. (A2),

$$X_{20} = \sqrt{\frac{3}{2}} (\cos^2 \theta - \frac{1}{3}), \quad (S_{ab})_{20} = \sqrt{\frac{3}{2}} (S_a^3 S_b^3 - \frac{1}{3} \vec{S}_a \cdot \vec{S}_b). \quad (\text{A4})$$

One can show the following relation between the Cartesian and spherical formulations,

$$X^{(2)ij} S_{ab}^{(2)ij} = \sum_{q=-2}^2 (-1)^q X_{2q} (S_{ab})_{2,-q} \equiv \vec{X}_2 \cdot (\vec{S}_{ab})_2, \quad (\text{A5})$$

which defines the scalar product of two rank-two spherical tensors [see Eq. (5.2.4) of Ref. [70]]. The spherical tensors \vec{X}_2 and $(\vec{S}_{ab})_2$ have spherical components X_{2q} and $(S_{ab})_{2q}$ for $q \in \{-2, -1, 0, 1, 2\}$. The \vec{X}_2 tensor acts (multiplicatively) on orbital angular momentum states. The tensor $(\vec{S}_{ab})_2$ acts on spin-angular momenta states. The total angular momentum is \vec{J} . Then, angular reduction according to Eq. (7.1.6) of Ref. [70] leads to

$$\langle LS'JJ_z | \vec{X}_2 \cdot (\vec{S}_{ab})_2 | LSJJ_z \rangle = (-1)^{L+S'+J} \left\{ \begin{matrix} J & S' & L \\ 2 & L & S \end{matrix} \right\} \langle L || \vec{X}_2 || L \rangle \langle S' || (\vec{S}_{ab})_2 || S \rangle. \quad (\text{A6})$$

One notes that, when $L = J$, the $6J$ symbol $\left\{ \begin{matrix} J & S' & L \\ 2 & L & S \end{matrix} \right\}$ has a nonvanishing off-diagonal element in spin space when $S' = 0$ and $S = 2$, and when $S' = 2$ and $S = 0$. The angular tensor \vec{X}_2 is proportional to the $L = 2$ spherical harmonic according to $X_{2q} = \sqrt{\frac{8\pi}{15}} Y_{2q}(\theta, \phi)$. Its reduced matrix element is

$$\langle L || \vec{X}_2 || L \rangle = \sqrt{\frac{2}{3}} (-1)^L (2L+1) \begin{pmatrix} L & 2 & L \\ 0 & 0 & 0 \end{pmatrix}. \quad (\text{A7})$$

The reduced matrix element for the single particle spin tensors (in states built from two spin-1 particles) is

$$\langle S' || (\vec{S}_{++})_2 || S \rangle = (-1)^S \sqrt{5} \Pi_{S'S} \left\{ \begin{matrix} S & S' & 2 \\ 1 & 1 & 1 \end{matrix} \right\}, \quad (\text{A8})$$

and

$$\langle S' || (\vec{S}_{--})_2 || S \rangle = (-1)^{S'} \sqrt{5} \Pi_{S'S} \left\{ \begin{matrix} S & S' & 2 \\ 1 & 1 & 1 \end{matrix} \right\}. \quad (\text{A9})$$

We have, according to Eqs. (A6), (A7), (A8) and (A9),

$$\begin{aligned} D_{LS'SJ} &\equiv \langle LS'JJ_z | (\hat{x}^i \hat{x}^j)^{(2)} [(S_+^i S_+^j)^{(2)} + (S_-^i S_-^j)^{(2)}] | LSJJ_z \rangle \\ &= \langle LS'JJ_z | \vec{X}_2 \cdot [(\vec{S}_{++})_2 + (\vec{S}_{--})_2] | LSJJ_z \rangle \\ &= (-1)^{S'+J} [(-1)^{S'} + (-1)^S] (2L+1) \sqrt{\frac{10}{3}} \Pi_{S'S} \left\{ \begin{matrix} J & S' & L \\ 2 & L & S \end{matrix} \right\} \begin{pmatrix} L & 2 & L \\ 0 & 0 & 0 \end{pmatrix} \left\{ \begin{matrix} S & S' & 2 \\ 1 & 1 & 1 \end{matrix} \right\}. \end{aligned} \quad (\text{A10})$$

The reduced matrix element of the mixed deuteron-antideuteron spin tensor can be written as

$$\langle S' || (\vec{S}_{+-})_2 || S \rangle = (-1)^{(S'+S)/2} \left(\frac{1 + \delta_{S'S}}{2} \right) \langle S' || [(\vec{S}_{++})_2 + (\vec{S}_{--})_2] || S \rangle. \quad (\text{A11})$$

It follows that

$$\begin{aligned} C_{LS'SJ} &\equiv \langle LS'JJ_z | (\hat{x}^i \hat{x}^j)^{(2)} (S_+^i S_-^j)^{(2)} | LSJJ_z \rangle = \langle LS'JJ_z | \vec{X}_2 \cdot (\vec{S}_{+-})_2 | LSJJ_z \rangle \\ &= (-1)^{(S'+S)/2} \left(\frac{1 + \delta_{S'S}}{2} \right) D_{LS'SJ}. \end{aligned} \quad (\text{A12})$$

-
- [1] C. J. Batty, *Antiprotonic-hydrogen atoms*, Rep. Prog. Phys. **52**, 1165–1216 (1989).
[2] E. Klempt, F. Bradamante, A. Martin, and J.-M. Richard, *Antinucleon–nucleon interaction at low energy:*

- scattering and protonium*, Phys. Rep. **368**, 119–316 (2002).
[3] K. Pachucki, *Electrodynamics of a compound system with relativistic corrections*, Phys. Rev. A **76**, 022106 (2007).

- [4] K. Pachucki, *Nuclear mass correction to the magnetic interaction of atomic systems*, Phys. Rev. A **78**, 012504 (2008).
- [5] J. Zatorski and K. Pachucki, *Electrodynamics of finite-size particles with arbitrary spin*, Phys. Rev. A **82**, 052520 (2010).
- [6] U. D. Jentschura and G. S. Adkins, *Quantum Electrodynamics: Atoms, Lasers and Gravity* (World Scientific, Singapore, 2022).
- [7] M. A. Proca, *Sur la théorie du positon*, C. R. Acad. Sci. Paris **202**, 1366–2368 (1936).
- [8] M. A. Proca, *Sur les équations fondamentales des particules élémentaires*, C. R. Acad. Sci. Paris **202**, 1490–1492 (1936).
- [9] R. J. Duffin, *On the Characteristic Matrices of Covariant Systems*, Phys. Rev. **54**, 1114 (1938).
- [10] N. Kemmer, *The particle aspect of meson theory*, Proc. Roy. Soc. London, Ser. A **173**, 91–116 (1939).
- [11] H. C. Corben and J. Schwinger, *The Electromagnetic Properties of Mesotrons*, Phys. Rev. **58**, 953–968 (1940).
- [12] J. A. Young and S. A. Bludman, *Electromagnetic Properties of a Charged Vector Meson*, Phys. Rev. **131**, 2326–2334 (1963).
- [13] D. E. Dorfan, J. Eades, L. M. Lederman, W. Lee, and C. C. Ting, *A Relativistic Equation for Bound-State Problems*, Phys. Rev. Lett. **14**, 1003–1006 (1965).
- [14] T. Massam, T. Muller, B. Righini, M. Schneegans, and A. Zichichi, *Experimental observation of antideuteron production*, Nuovo Cimento **39**, 10–14 (1965).
- [15] R. Caravita, *Perspectives from a cold antideuteron beam in the AD/ELENA facility*, e-print arXiv:2404.08000v1.
- [16] P. Blumer, B. Ohayon, and P. Crivelli, *Production and study of antideuteronium with the GBAR beamlines*, Eur. Phys. J. D **79**, 17 (2025).
- [17] T. Nebel, F. D. Amaro, A. Antognini, F. Biraben, J. M. R. Cardoso, C. A. N. Conde, A. Dax, S. Dhawan, L. M. P. Fernandes, A. Giesen, T. Hänsch, P. Indelicato, L. Julien, P. E. Knowles, F. Kottmann, E. Le Bigot, Y.-W. Liu, J. A. M. Lopes, L. Ludhova, C. M. B. Monteiro, F. Mulhauser, F. Nez, R. Pohl, P. Rabinowitz, J. M. F. dos Santos, L. A. Schaller, K. Schuhmann, C. Schwob, D. Taqq, and J. F. C. A. Veloso, *Highly coherent, Watt-level deep-UV radiation via a frequency-quadrupled Yb-fiber laser system*, Can. J. Phys. **85**, 469–478 (2007).
- [18] E. A. Uehling, *Polarization Effects in the Positron Theory*, Phys. Rev. **48**, 55 (1935).
- [19] G. Källén and A. Sabry, *Fourth Order Vacuum Polarization*, Kong. Dan. Vid. Sel. Mat. Fys. Med. **29**, 1–20 (1955).
- [20] S. Laporta and U. D. Jentschura, *Dimensional Regularization and Two-Loop Vacuum Polarization Operator: Master Integrals, Analytic Results and Energy Shifts*, Phys. Rev. D **109**, 096020 (2024).
- [21] S. Deser, M. L. Goldberger, K. Baumann, and W. Thirring, *Energy level displacements in pi-mesonic atoms*, Phys. Rev. **96**, 774–776 (1954).
- [22] H. A. Bethe and F. de Hoffmann, *Mesons and fields, Vol. 2* (Row, Peterson and Co., Evanston, IL, 1955).
- [23] N. Byers, *Interactions of low-energy negative pions with nuclei*, Phys. Rev. **107**, 843–849 (1957).
- [24] T. L. Trueman, *Energy level shifts in atomic states of strongly-interacting particles*, Nucl. Phys. **26**, 57–67 (1961).
- [25] G. S. Adkins and U. D. Jentschura, *Short-Range Hard-Sphere Potential and Coulomb Interaction: Generalized Deser–Trueman Formula*, submitted (2025).
- [26] E. Tiesinga, P. J. Mohr, D. B. Newell, and B. N. Taylor, *CODATA recommended values of the fundamental physical constants: 2018*, Rev. Mod. Phys. **93**, 025010 (2021).
- [27] P. J. Mohr, D. B. Newell, B. N. Taylor, and E. Tiesinga, *CODATA recommended values of the fundamental physical constants: 2022*, Rev. Mod. Phys. **97**, 025002 (2025).
- [28] M. Puchalski, J. Komasa, and K. Pachucki, *Hyperfine structure of the first rotational level in H_2 , D_2 and HD molecules and the deuteron quadrupole moment*, Phys. Rev. Lett. **125**, 253001 (2020).
- [29] J. M. B. Kellogg, I. I. Rabi, N. F. Ramsey, and J. R. Zacharias, *An Electric Quadrupole Moment of the Deuteron*, Phys. Rev. **55**, 318–319 (1939).
- [30] J. M. B. Kellogg, I. I. Rabi, N. F. Ramsey, and J. R. Zacharias, *An Electric Quadrupole Moment of the Deuteron*, Phys. Rev. **57**, 677–695 (1940).
- [31] J. J. Krauth, M. Diepold, B. Franke, A. Antognini, F. Kottmann, and R. Pohl, *Theory of the $n = 2$ levels in muonic deuterium*, Ann. Phys. (N.Y.) **366**, 168–196 (2016).
- [32] G. S. Adkins and U. D. Jentschura, *Relativistic and Recoil Corrections to Light-Fermion Vacuum Polarization for Spin-1 Bound Systems*, in preparation for Phys. Rev. A (2025).
- [33] G. S. Adkins and U. D. Jentschura, *Deuteronium (Deuteron–Antideuteron Bound System Higher-Order Radiative Corrections and Sensitivity to Hidden Interactions)*, submitted (2025).
- [34] V. B. Berestetskii, E. M. Lifshitz, and L. P. Pitaevskii, *Quantum Electrodynamics, Volume 4 of the Course on Theoretical Physics*, 2 ed. (Pergamon Press, Oxford, UK, 1982).
- [35] J. Schwinger, *Particles, Sources and Fields (Volume III)* (Addison-Wesley, Reading, MA, 1970).
- [36] G. Pustovalov, *Vacuum polarization in Mesonic Atoms*, Zh. Éksp. Teor. Fiz. **32**, 1519 (1957), [JETP **5**, 1234 (1957)].
- [37] S. Wolfram, *The Mathematica Book*, 4 ed. (Cambridge University Press, Cambridge, UK, 1999).
- [38] D. A. Owen and W. W. Repko, *Vacuum-Polarization Corrections to the Hyperfine Structure of the $\mu^+\mu^-$ Bound System*, Phys. Rev. A **5**, 1570–1572 (1972).
- [39] K. Pachucki, *Theory of the Lamb shift in muonic hydrogen*, Phys. Rev. A **53**, 2092–2100 (1996).
- [40] U. D. Jentschura, G. Soff, V. G. Ivanov, and S. G. Karshenboim, *Bound $\mu^+\mu^-$ system*, Phys. Rev. A **56**, 4483–4495 (1997).
- [41] S. G. Karshenboim, V. G. Ivanov, U. D. Jentschura, and G. Soff, *Bound states of the muon-antimuon system: lifetimes and hyperfine splitting*, JETP **86**, 226–236 (1998), [ZhETF JETP **113**, 409 (1998)].
- [42] E. Borie, *Lamb Shift in Light Muonic Atoms–Revisited*, Ann. Phys. (N.Y.) **327**, 733–763 (2012).
- [43] S. G. Karshenboim, V. G. Ivanov, and E. Y. Korzinin, *Relativistic recoil corrections to the electron-vacuum-polarization contribution in light muonic atoms*, Phys. Rev. A **85**, 032509 (2012).
- [44] W. W. Repko and D. A. Dicus, *Muonic hydrogen and the proton size*, Phys. Rev. D **98**, 013002 (2018).
- [45] W. W. Repko and D. A. Dicus, *Relativistic corrections to vacuum polarization contributions in muonic hydrogen*,

- Phys. Rev. D **98**, 033006 (2018).
- [46] U. D. Jentschura, *Lamb Shift in Muonic Hydrogen. —I. Verification and Update of Theoretical Predictions*, Ann. Phys. (N.Y.) **326**, 500–515 (2011).
 - [47] J. Schwinger, *Particles, Sources and Fields (Volume II)* (Addison-Wesley, Reading, MA, 1970).
 - [48] B. R. Johnson and J. O. Hirschfelder, *The radial reduced Coulomb Green's function*, J. Math. Phys. **20**, 2484–2501 (1979).
 - [49] B. R. Johnson, private communication (2023).
 - [50] B. J. Laurenzi and A. Flamberg, *Electronic computation of first-order wave functions using Green's functions*, Int. J. Quantum Chem. **11**, 869–880 (1977).
 - [51] G. J. Gounaris and J. J. Sakurai, *Finite-width corrections to the vector-meson-dominance prediction for $\rho \rightarrow e^+e^-$* , Phys. Rev. Lett. **21**, 244–247 (1968).
 - [52] J. R. Sapirstein, E. A. Terray, and D. R. Yennie, *Radiative-recoil corrections to muonium and positronium hyperfine splitting*, Phys. Rev. D **29**, 2290 (1984).
 - [53] S. Navas *et al.* [Particle Data Group], *Review of Particle Physics*, Phys. Rev. D **110**, 030001 (2024).
 - [54] T. H. Bauer, R. D. Spital, D. R. Yennie, and F. M. Pipkin, *The hadronic properties of the photon in high-energy interactions*, Rev. Mod. Phys. **50**, 261 (1978), [Erratum Rev. Mod. Phys. **51**, 407 (1979)].
 - [55] A. Keshavarzi, D. Nomura, and T. Teubner, *Muon $g - 2$ and $\alpha(M_Z^2)$: A new data-based analysis*, Phys. Rev. D **97**, 114025 (2018).
 - [56] B. E. Lautrup, A. Petermann, and E. de Rafael, *Recent developments in the comparison of theory and experiment in quantum electrodynamics*, Phys. Rep. **3C**, 193 (1972).
 - [57] S. L. Adler, *Some simple vacuum-polarization phenomenology: $e^+e^- \rightarrow$ hadrons; the muonic-atom x -ray discrepancy and $g_\mu - 2$* , Phys. Rev. D **10**, 3714–3728 (1974).
 - [58] R. Barbieri, J. A. Mignaco, and E. Remiddi, *Electron Form Factors up to Fourth Order. -I*, Nuovo Cimento **11**, 824–864 (1972).
 - [59] J. L. Friar and G. L. Payne, *Deuteron dipole polarizabilities and sum rules*, Phys. Rev. C **72**, 014004 (2005).
 - [60] J. D. Jackson, *Classical Electrodynamics*, 3 ed. (J. Wiley & Sons, New York, NY, 1998).
 - [61] U. D. Jentschura, *Revisiting the Divergent Multipole Expansion of Atom–Surface Interactions: Hydrogen and Positronium, α -Quartz, and Physisorption*, Phys. Rev. A **109**, 012802 (2024).
 - [62] N. L. Rodning, L. D. Knutson, W. G. Lynch, and M. B. Tsang, *Measurement of the electric polarizability of the deuteron*, Phys. Rev. Lett. **49**, 909–912 (1982).
 - [63] J. L. Friar, S. Fallieros, E. L. Tomusiak, D. Skopik, and E. G. Fuller, *Electric polarizability of the deuteron*, Phys. Rev. C **27**, 1364(R)–1366(R) (1983).
 - [64] K. V. Protasov, G. Bonomi, E. Lodi Rizzini, and A. Zenoni, *Antiproton annihilation on light nuclei at very low energies*, Eur. Phys. J. A **7**, 429–434 (2000).
 - [65] S. Berko and H. N. Pendleton, *Positronium*, Annu. Rev. Nucl. Part. Sci. **30**, 543–581 (1980).
 - [66] S. G. Karshenboim, *Precision study of positronium: Testing bound state QED theory*, Int. J. Mod. Phys. A **19**, 3879–3896 (2004).
 - [67] G. S. Adkins, D. B. Cassidy, and J. Pérez-Ríos, *Precision spectroscopy of positronium: Testing bound-state QED theory and the search for physics beyond the Standard Model*, Phys. Rep. **975**, 1–61 (2022).
 - [68] S. G. Karshenboim, U. D. Jentschura, V. G. Ivanov, and G. Soff, *Next-to-leading and higher order corrections to the decay rate of dimuonium*, Phys. Lett. B **424**, 397–404 (1998).
 - [69] S. J. Brodsky and R. F. Lebed, *Production of the Smallest QED Atom: True Muonium ($\mu^+ \mu^-$)*, Phys. Rev. Lett. **102**, 213401 (2009).
 - [70] A. R. Edmonds, *Angular Momentum in Quantum Mechanics* (Princeton University Press, Princeton, New Jersey, 1957).